National Aeronautics and Space Administration

Composite Assisted Funneling of Electrons for Improved Performance of Bulk Thermoelectric Materials

Principal Investigator: James Minh Ma (3464)

Paul von Allmen (3980), Sergey V. Prikhodko (UCLA), Trinh Vo (398K), Richard B. Kaner (UCLA), Sabah K. Bux (3464), Jean-Pierre Fleurial (3464)

Introduction

Thermoelectric materials convert heat to electricity through the Seebeck effect

- Heat flow drives charge carriers from hot side to cold side

Ideal spacecraft power source for:

- Long mission lives
- High dust environments
- Lack of solar radiation due to distance from sun, geological obstructions, high/low latitudes

Historically ≤ 6.5% efficiency

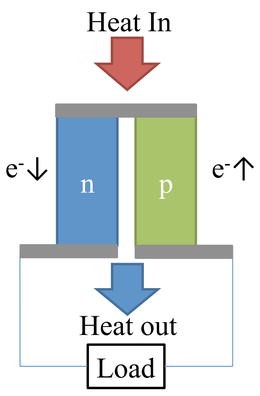

Thermoelectric generator on Curiosity

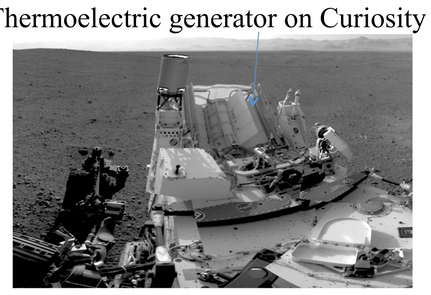

TE conversion efficiency a function of hot junction T, ΔT, and ZT

$$\eta_{max} = \frac{T_{hot} - T_{cold}}{T_{hot}} \cdot \frac{\sqrt{1+ZT} - 1}{\sqrt{1+ZT} + \frac{T_{cold}}{T_{hot}}}$$

Thermoelectric Figure of Merit

$zT = S^2 \sigma / \rho k \, T$

S, Seebeck coefficient (μV/K)
ρ , electrical resistivity (mohm cm)
k, thermal conductivity (mW/cmK)
T, temperature (K)

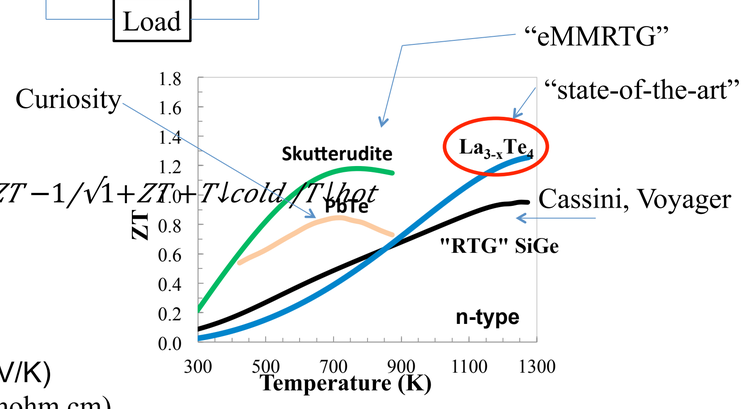

Maximized area under curve = high efficiency

Objective: Utilize Composites to Combine Positive Attributes of Different Materials to Increase zT

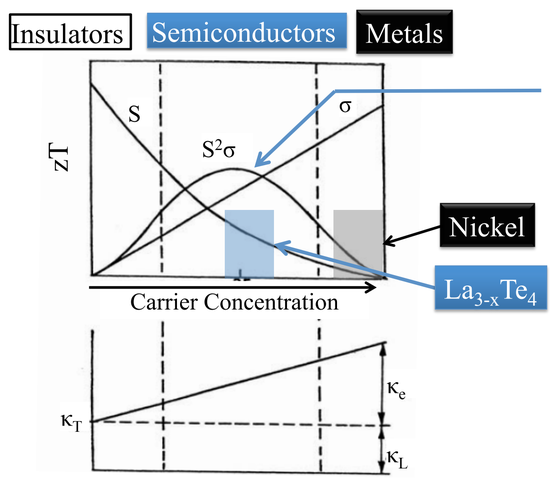

Traditional thermoelectrics are a compromise of transport properties to optimize zT

Composite state-of-the-art thermoelectric lanthanum telluride, $La_{3-x}Te_4$, with nickel metal to lower electrical resistivity and increase zT

Methods

Mechanochemical synthesis from the elemental La + Te

Crystalline $La_{3-x}Te_4$ powder synthesized in the ball mill

$La_{3-x}Te_4$ combined with nickel powder

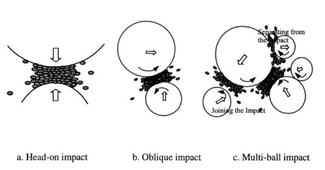

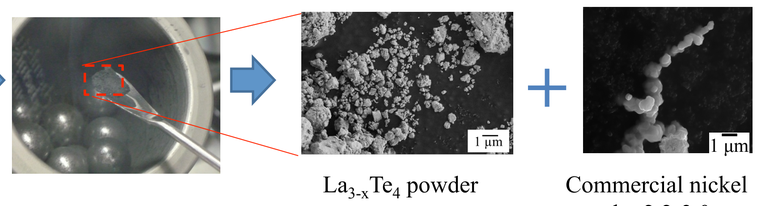

$La_{3-x}Te_4$ powder

Commercial nickel powder 2.2-3.0 μm avg. particle size

X-ray diffraction shows only $La_{3-x}Te_4$ and Ni phase

> 99% density pellets

Sinter using Spark Plasma Sintering

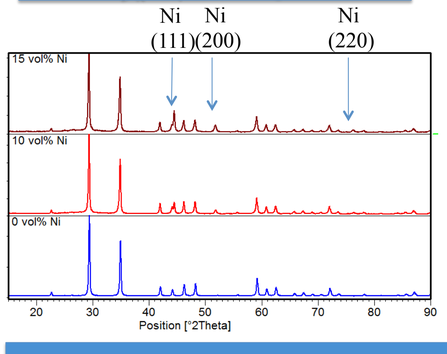

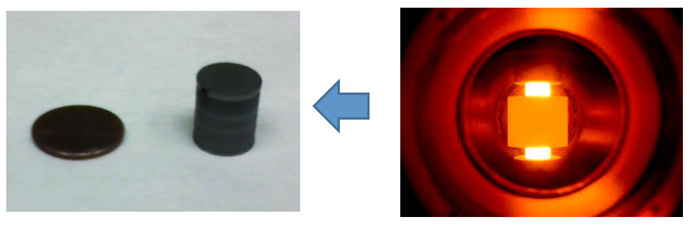

A typical 12.6 mm O.D. sample compared to a penny

The scope of this study was to examine the effect of nickel volume fraction upon zT and the transport properties

Results

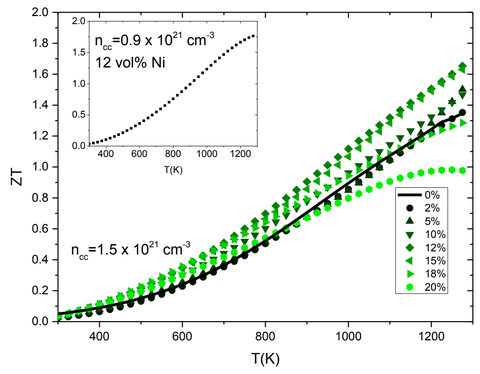

Increasing nickel loading

0-10 vol%	10-15 vol%	> 15 vol%
• No change	• 25% ↑ zT	• ↓ zT

Optimizing $La_{3-x}Te_4$-Ni to a lower carrier concentration leads to a 50% improvement over previously reported zT

Transport Properties

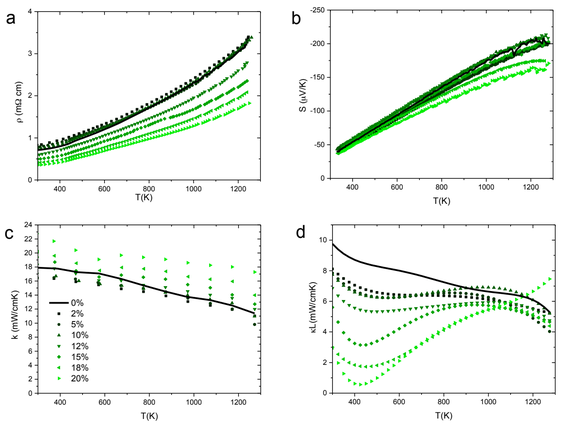

	<10 vol%	10-15 vol%	> 15 vol%
ρ, electrical resistivity	No change	↓	↓
S, Seebeck	No change	No change	↓
κ, thermal conductivity	No change	No change	↑
zT	No change	↑	↓

10-15 vol% window where electrical resistivity is decoupled from Seebeck and κ allowing for increased zT

Proposed Mechanism: Composite Assisted Funneling of Electrons in $La_{3-x}Te_4$ (CAFE LaTe) allows for increased zT

Increasing nickel metal loading results in extended nickel networks

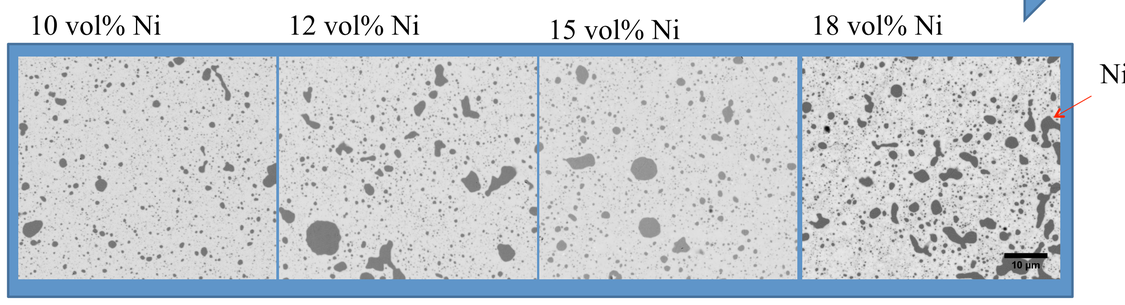

Electron funneling through low resistivity metal network lowers resistivity

Monte Carlo Simulation of $La_{3-x}Te_4$-Ni

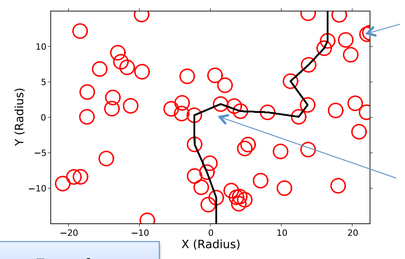

Nickel inclusions

Low resistance paths form when distance to nearest neighbor <4.4x the inclusion radius

Increased current density through low resistance paths

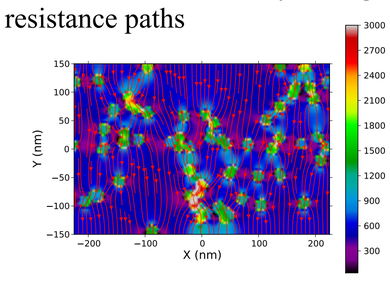

Conclusions

- Composite Assisted Funneling of Electrons utilizes a network of metal inclusions to lower electrical resistivity of a thermoelectric matrix enhancing zT
- CAFE $La_{3-x}Te_4$ exhibits a +25% in zT_{max} compared $La_{3-x}Te_4$ and +80% over heritage "RTG" SiGe
- Increase in zT_{avg} = 1.3 (+25%) for T = 875 K – 1275 K
- CAFE $La_{3-x}Te_4$ exhibits the highest reported zT in the temperature range of 1000 - 1275 K
- Potential to apply the CAFE technique to improve the zT of other thermoelectric materials

Acknowledgements

The work described here was carried out at the Jet Propulsion Laboratory, California Institute of Technology, under contract with the National Aeronautics and Space Administration. This work supported by the NASA Science Missions Directorate's Radioisotope Power Systems Thermoelectric Technology Development Project

Select References

1. Ma, J. M., Allmen P. v., Prikhodko, S. V., Vo, T., Kaner, R. B., Bux, S. K., Fleurial, J. P.; Submitted *Nature Materials* 2015
2. May, A., Fleurial, J. & Snyder, G. Thermoelectric performance of lanthanum telluride produced via mechanical alloying. *Phys. Rev. B* **78,** 1–12 (2008).
3. Bergman, D. J. & Fei, L. G. Enhancement of thermoelectric power factor in composite thermoelectrics. *J. Appl. Phys.* **85,** 8205–8216 (1999).
4. Snyder, G. J. & Toberer, E. S. Complex thermoelectric materials. *Nat Mater* 7, 105–114 (2008).

Poster No. T2

National Aeronautics and Space Administration
Jet Propulsion Laboratory
California Institute of Technology
Pasadena, California

www.nasa.gov

National Aeronautics and Space Administration

NanoSpacecraft for the Exploration of Small Bodies

Principal Investigator – Simon Tardivel (312)
NPP Advisor – Andrew T. Klesh (312)

Small Bodies

Planetary defense, human exploration, in-situ resource utilization, science : small bodies have become prime space exploration targets.

Unlike planets or moons, small bodies present odd hazards but are also relatively easy to explore - they have very low mass. This makes them ideal targets for NanoSpacecraft (1 - 25 kg, 1 - 15 L).

NanoSats and NanoLanders

Two promising mission architectures were identified and investigated for feasibility and science return.

- **Lone NanoSat**: a self-propelled NanoSpacecraft travels from Earth to an asteroid or comet, and performs a science mission

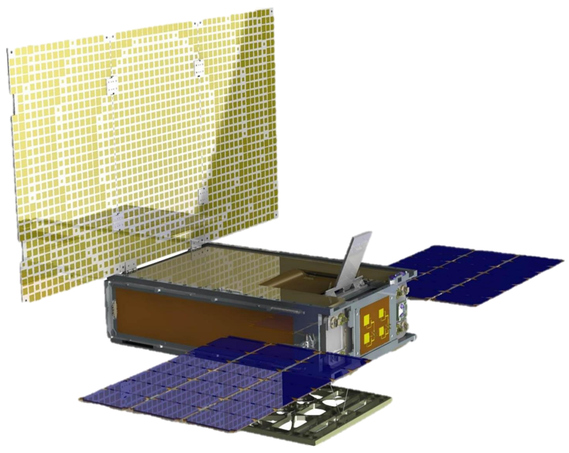

Courtesy of NASA/JPL

Mars Cube One (MarCO) weighs only 14 kg
but will travel alongside InSight, to Mars, in 2016.
A similar NanoSat could rendezvous with an asteroid.

- **NanoLander**: a NanoSpacecraft is given a ride by a larger mothership and is deployed to the surface

Courtesy of DLR

The NanoLander Mascot weighs only 10 kg, but it is already en route to 1999 JU3 aboard Hayabusa 2.
Some instruments are miniature versions of Philae's.

Conclusions

Lone NanoSats make possible and affordable an in-situ survey of asteroids – comets are difficult to rdv.

- Escape velocity provided by a launch vehicle
- Many accessible targets exist
- Focused science opportunities exist

Future work: GNC, operations complexity, costing.

NanoLanders are a great and inexpensive asset for any large mothership visiting an asteroid.

- We have a safe, easy, reliable deployment strategy.
- Containerized payload allows for safe isolation
- They can acquire ground truth and in-situ data

Future work: surface interaction, power generation.

Lone NanoSats

Existing deep space CubeSat hardware, such as INSPIRE and MarCO, provides a basis for the design of an Asteroid CubeSat Explorer (ACE) aiming for targets of opportunity (1-3 available/yr)

System	Notes	Mass
Bus	6U CubeSat	4.0 kg
Power	solar arrays 35W @1AU (2x3x7 cells)	1.5 kg
Propulsion	electrospray 0.7 mN (for 15W and Isp≈800 s)	1.0 kg
ACS	flywheels, RCS thrusters, star-tracker, sun sensor	2.0 kg
Telecom	HGA (reflect array), LGA	2.0 kg
Payload	camera, small instrument	0.5 kg
Propellant	650m/s for electrospray + 2 years RCS desaturation	1.5 kg
TOTAL	**ASTEROID CUBESAT EXPLORER**	**12.5 kg**

- **Propulsion technology**: new electric propulsion designs (e.g. electrospray) give NanoSats real propulsive abilities at TRL 5+. But, launch insertion to Earth escape is still required. The subsystems that would allow a NanoSat to escape on its own do not yet exist. Limitations include power usage, thermal control, radiation shielding, propellant volume, thruster lifetime, etc.

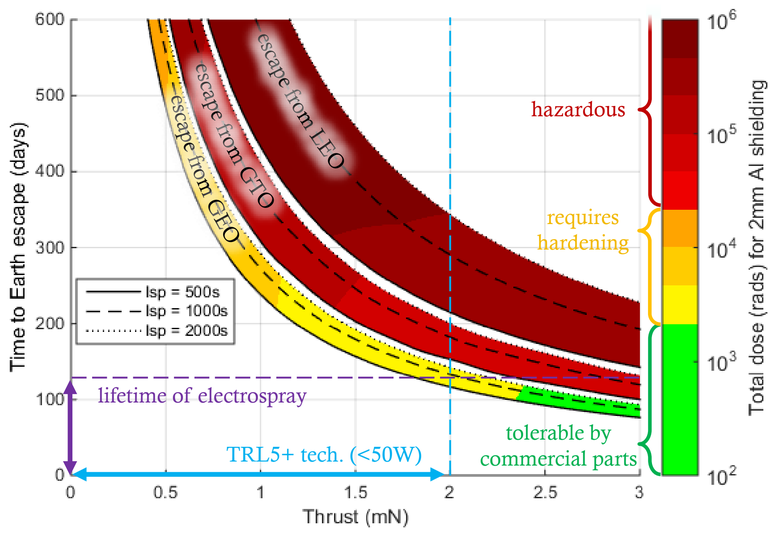

Time of transfer and accumulated dose, from LEO, GTO, or GEO to Earth's escape, for 3 different Isp, as a function of (low) thrust.

- **Maneuverability:** we determine the capabilities of the lone NanoSat by comparing to past mission's spacecraft.

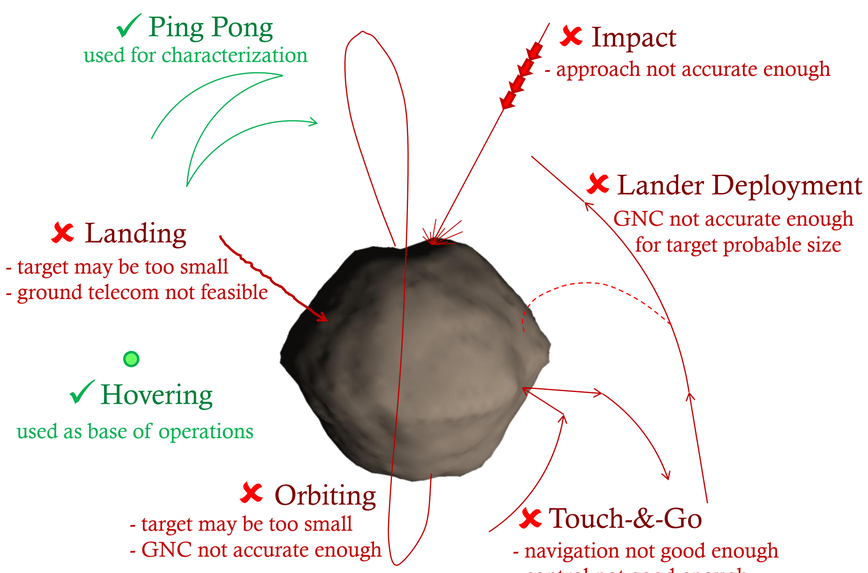

A lone NanoSat has limited capabilities, but can still rendezvous. Some maneuvers are possible ✓, some are areas of technology development ✘, especially for local GNC.

Using radio science, its navigation camera, and another, small payload (e.g. I.R. camera), the NanoSat can then answer:

- What are the basic asteroid physical properties?
- How does this asteroid compare to previously visited bodies?

NanoLanders

We designed a strategy for the deployment of NanoLanders from a mothership. It has limited risk for the mothership, and the lander does not use any thrusters or active landing platform (e.g. harpoons):

- The mothership is inserted on a low-speed hyperbolic trajectory
- The mothership flies by a saddle equilibrium point of the system
- The lander is jettisoned on the go, near this point
- The lander falls passively to the surface and bounces several times before coming to rest

To validate this strategy, our simulations use high-fidelity gravity fields and very detailed modeling of the surface interaction – from the global shape of the asteroid to the presence of 10 cm rocks.

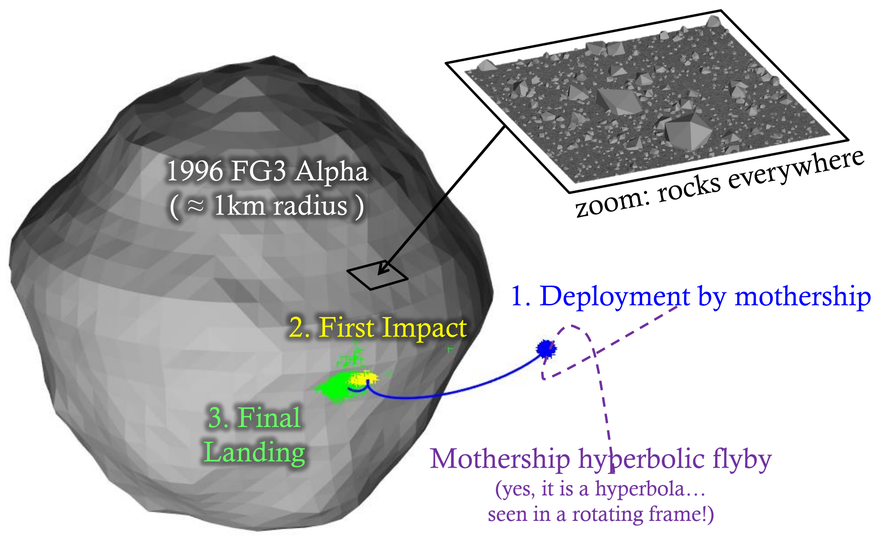

Simulations of a safe and optimized deployment of a spherical NanoLander on the fast spinning asteroid 1996 FG3 Alpha.

Designed for the BASiX mission proposal, this strategy shows rates of success higher than 99.7%, even on challenging targets and with coarse GNC. Many practical case studies were and are considered:

- Mascot, aboard Hayabusa 2, that will reach 1999 JU3 in 2018
- Geopods (BASiX), Mascot2 (AIM), Fantina (MarcoPoloR)

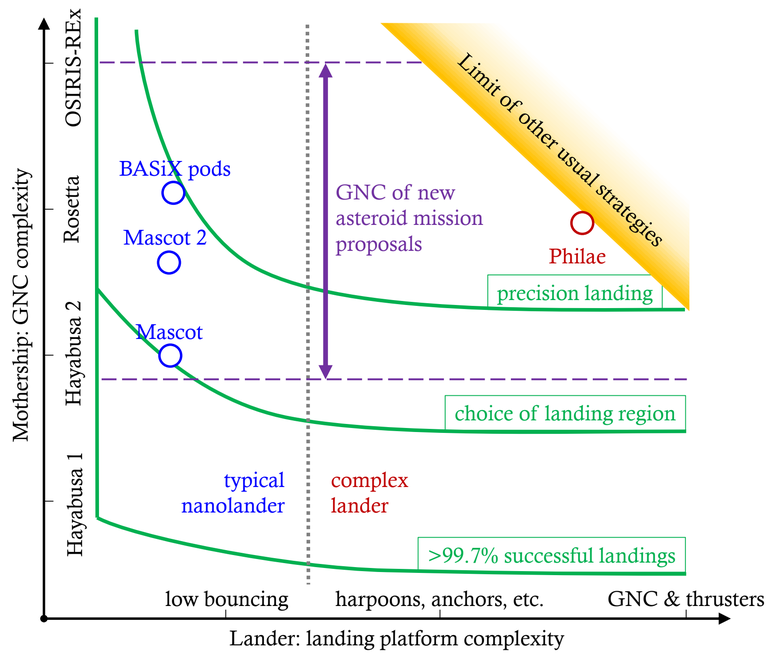

This graphs summarizes the capabilities of our strategy:
contrary to other usual landing strategies,
it enables simple, cheap and efficient NanoLanders.

Once on the surface, a NanoLander can survive on batteries for some payloads, or utilize solar panels if need be. It can be static, or use a mobility mechanism, like Mascot which can rotate and hop.

Contrary to the lone NanoSat, the NanoLander has a high payload/platform ratio (30% for Mascot). A considerable effort has been made by the community to accommodate nanoscale instruments: cameras, radar tomographers, mass spectrometers, etc.

National Aeronautics and Space Administration

Jet Propulsion Laboratory
California Institute of Technology
Pasadena, California

www.nasa.gov

Looking for references or further reading?
Ask me for a bibliography!

Poster No. T-4

National Aeronautics and Space Administration

The Cold Atom Laboratory (CAL) mission

Principal Investigators: Markus Krutzik and Ethan Elliott (332J)

David Aveline (332J), Robert Thompson (332J), Nan Yu (332J), and the CAL team

From Quantum to Cosmos

Cold atoms - an enabling technology

Over one hundred experiments in ultracold quantum gases are spread across the globe. Cold atom research led to **3 Nobel prizes in physics**, honoring the creation of new states of matter and the most precise quantum sensors currently known.

The Cold Atom Laboratory (CAL) is a **multi-user facility** that will allow the first study of ultracold quantum gases in the micro-gravity condition of the International Space Station (ISS).

In this force-free environment, CAL could advance not only Earth observation, navigation, and metrology, but also our ability to address some of the most fundamental - and still unsolved - questions of modern physics: **What is the source of the dis-agreement between quantum mechanics and classical gravity?**

Quantum sensors in space - a versatile testbed for fundamental and applied physics

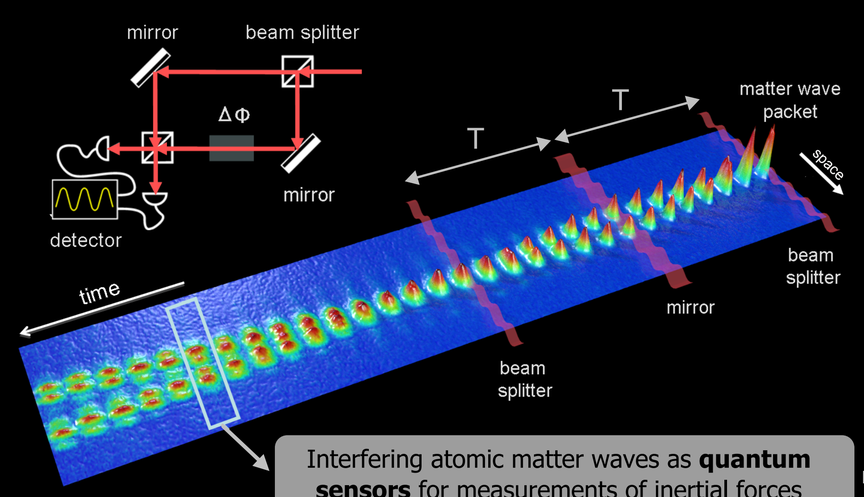

Interfering atomic matter waves as **quantum sensors** for measurements of inertial forces

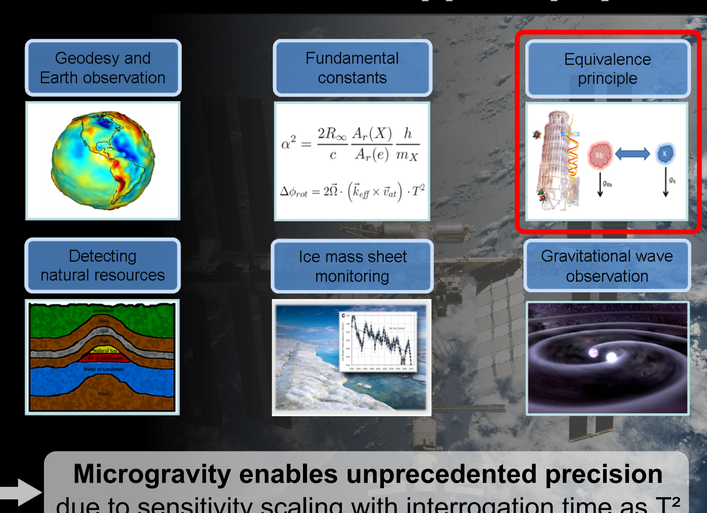

Microgravity enables unprecedented precision due to sensitivity scaling with interrogation time as T^2

Ultracold Atom Generation

The CAL instrument: miniaturizing the production of ultracold atoms

4. Magnetic chip trap: contain and evaporate atoms to a billionth of a degree above absolute zero (miniaturized current carrying gold wires)

3. Laser systems: cool atoms in 3D and load magnetic trap

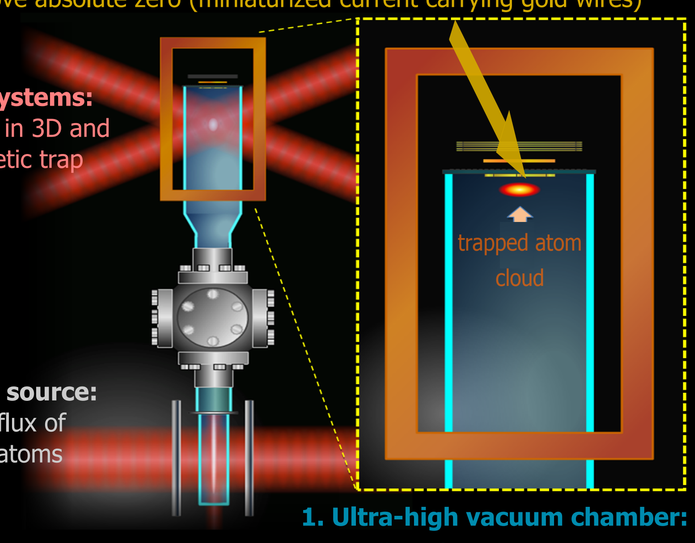

2. Atomic source: controlled flux of precooled atoms

Picture adapted from Anderson group, University of Colorado, Boulder

1. Ultra-high vacuum chamber: thermally isolate the atoms

Observing clouds of ultracold atoms with **absorption imaging techniques**

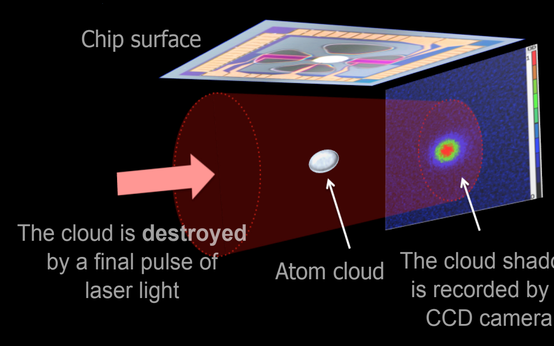

Instrument reliability: the system must recreate atomic clouds with the same initial conditions for **every** picture

The Bose-Einstein condensate (BEC)

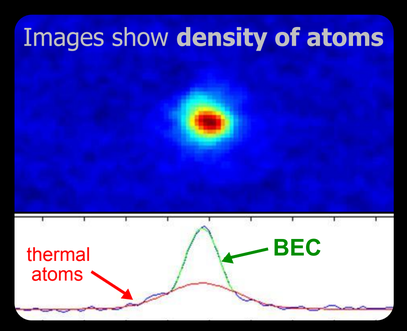

This regime is **only achievable in a microgravity environment**

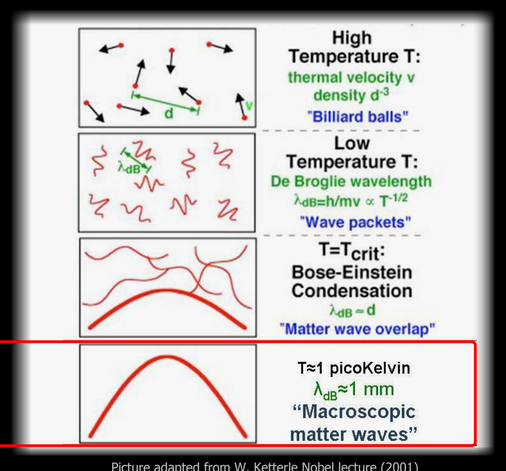

Picture adapted from W. Ketterle Nobel lecture (2001)

As the temperature drops, the density abruptly spikes, indicating a collection of **overlapped matter waves** and phase transition into a BEC: **The ideal quantum probe for space applications**

CAL's Ground Testbed Results

Hardware development and critical technology validation

We have developed two independent quantum gas experiments for the CAL ground testbed, one Rubidium BEC system and one designed for Rubidium and Potassium. They **each** require the following subsystems:

Laser sources and electronics

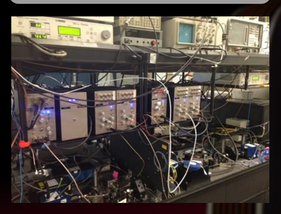

Light generation and stabilization for laser cooling, atomic state preparation, and detection

Control system and power supplies

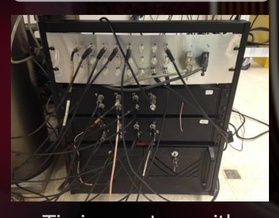

Timing system with 16 analog and 24 digital channels to control the experimental sequence

RF and microwave distribution

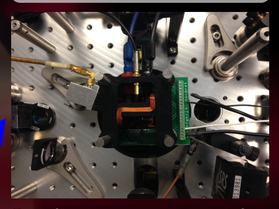

Synthesizers, waveguides and antennas for selective rejection of trapped atoms (evaporation)

Light distribution and switching

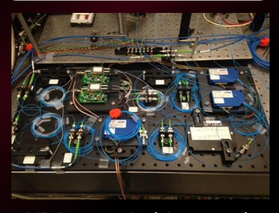

Mixing, switching, and distribution of different laser frequencies

Physics package

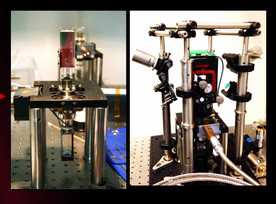

UHV environment, magnetic fields, and optomechanics for BEC generation

electrical interface
optical interface

Observation of BECs and dual-species mixtures at JPL

We have succesfully generated (i) the first BEC in CAL's ground testbed, (ii) the first Rb and K dual species 2D MOT, 3D MOT and trapped mixtures at JPL, and (iii) the **world's first generation of a BEC with microwaves on an atom chip**.

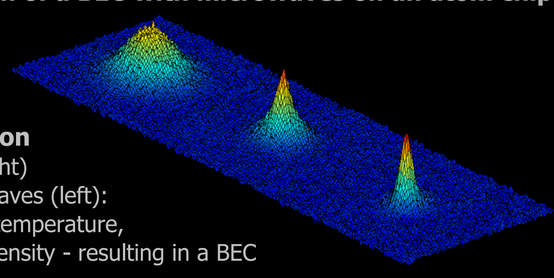

Evaporation with RF (right) and microwaves (left): **Decrease** temperature, **increase** density - resulting in a BEC

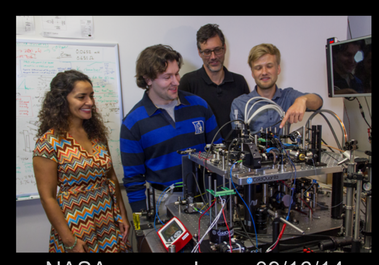

NASA news release 09/16/14

A critical milestone towards dual species BECs was reached April 2015: **World's first chip-based microwave BEC achieves the same performance as RF BEC**

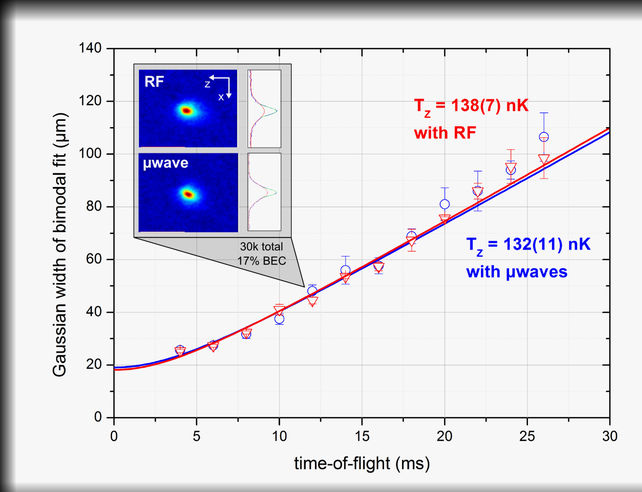

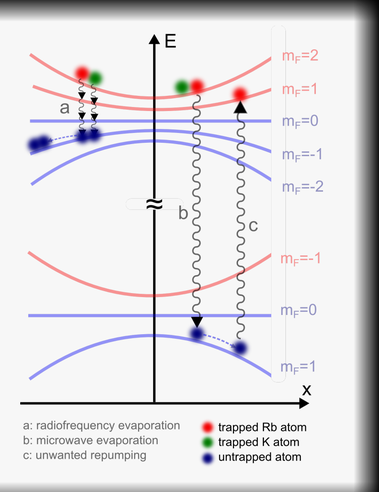

National Aeronautics and Space Administration

Jet Propulsion Laboratory
California Institute of Technology
Pasadena, California

www.nasa.gov

Poster No. T-6

GeoSTAR III Preliminary Validation Test Results

Isaac Ramos-Perez (382G)
Todd C. Gaier, Pekka P. Kangaslahti, Alan B. Tanner (382G)
Bjorn Lambrigtsen (329M)

National Aeronautics and Space Administration

Motivation and Objective: The Geostationary Synthetic Thinned Aperture Radiometer (GeoSTAR) was developed to fill the absence of microwave atmospheric sounder in geostationary orbit with continuous views of the entire visible Earth disc. GeoSTAR is important for observation of hurricanes and strong storms in all-weather conditions. The current laboratory prototype of GeoSTAR III is a Y-shaped array of 144 elements operating at millimeter-wave water vapor absorption line (165-183 GHz region). The objective of this work is to test the individual parts before assembly in the subsystems, focus in a method using correlation techniques to test the noise figure, gain, and I/Q phase quadrature of the MIniature MMIC low mass/power RAdiometer Module (MIMRAM) modules with only one measurement.

GeoSTAR III block diagram

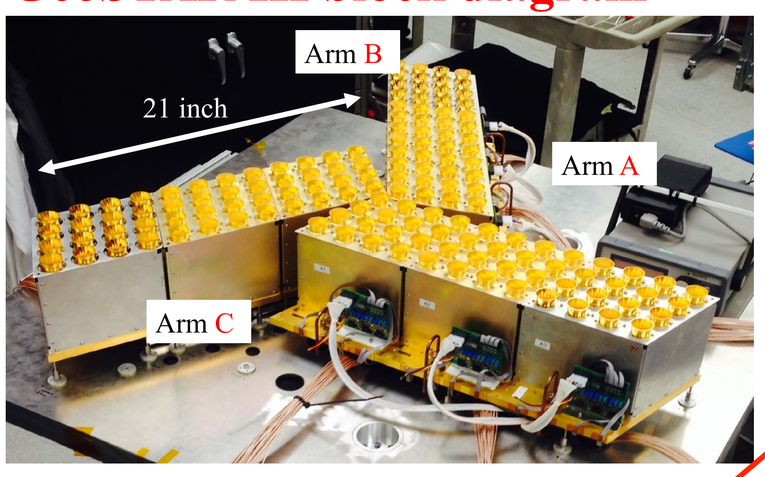

Array of 144 antennas with 288 outputs (I and Q)

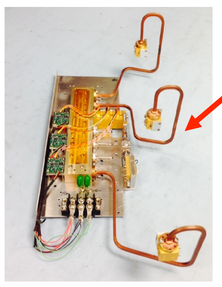

LO WR-10 Power divider 1:6 x 3 units

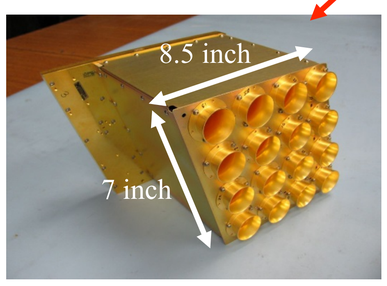

Manifold x 9 units

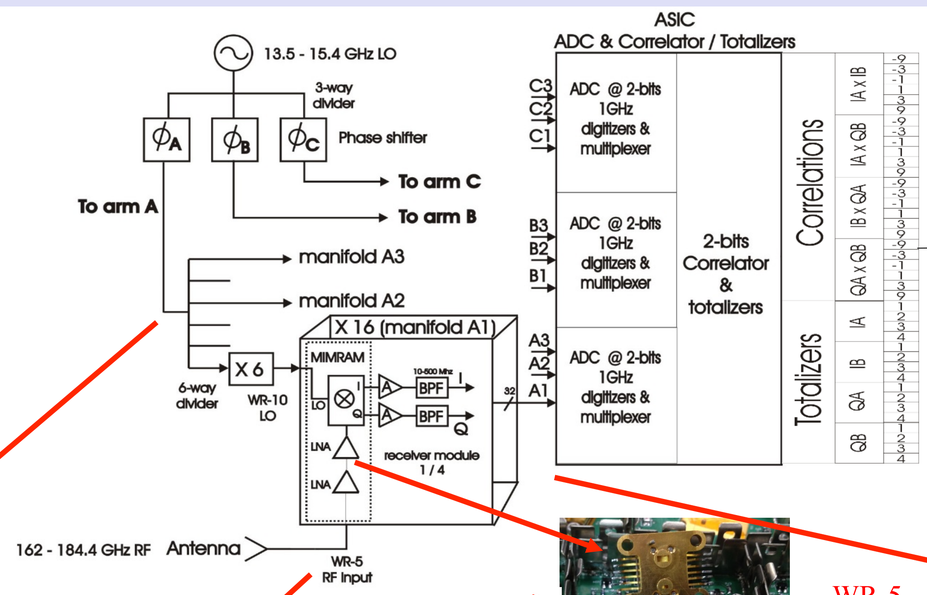

ASIC Correlator

- Technology matured in this program
- 500 MHz bandwidth
- 2 bit ADC correlator
- Number of correlator ~ 200,000 (*)

(*) Space instrument 384 elements with 128^2 X 4 products X 3 arms

- DC power correlator system < 100 W

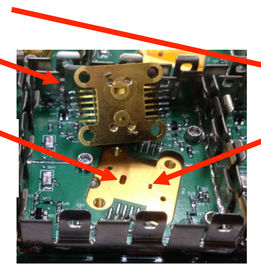

MIMRAM waveguide interface

- Technology matured in this program
- Receiver with low noise, reduced size, mass and power
- In-phase and quarture signals

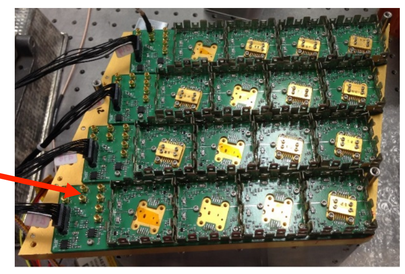

Manifold bottom part with IF boards x 36 units
36 board x 4 = 144 MIMRAMs and MIMRAMs

MIMRAM's characterization test setup

Challenge: Characterization the basic receiver in terms of (I-Q, G, NF) with a single measurement. It is **ideal for measurement of a large number of devices**.

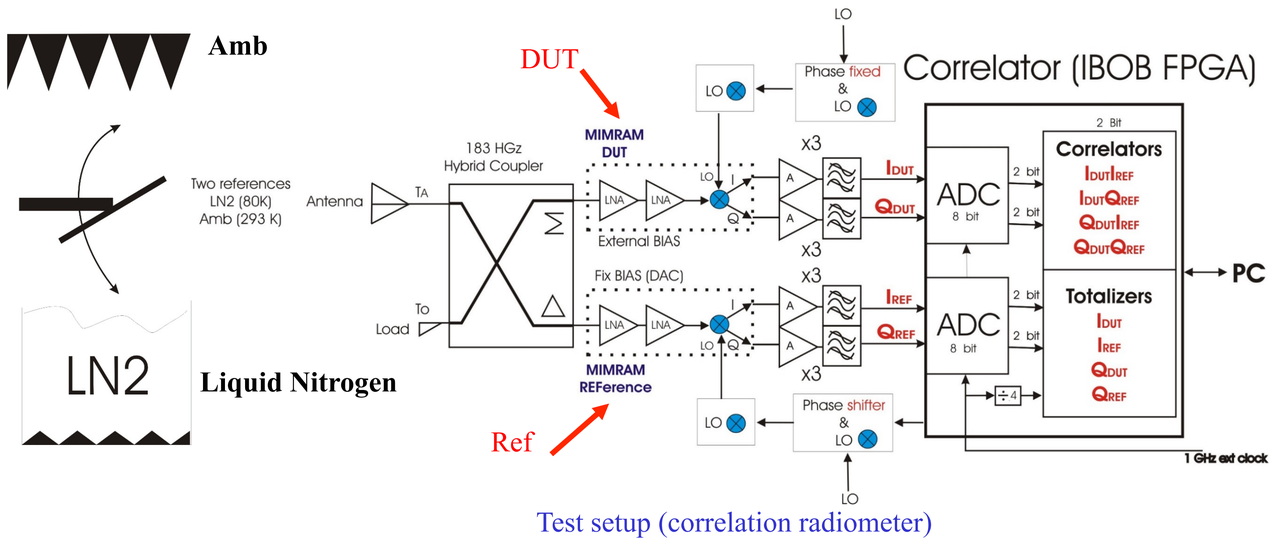

Test setup (correlation radiometer)

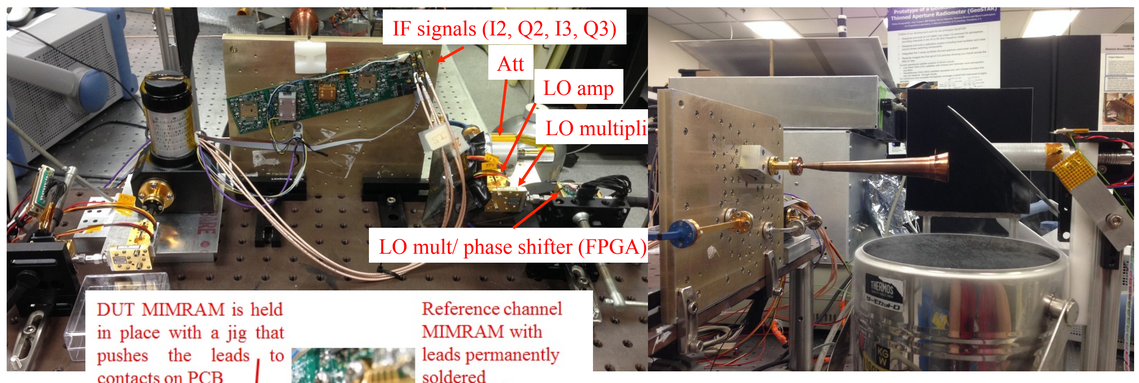

144 MIMRAMs to test

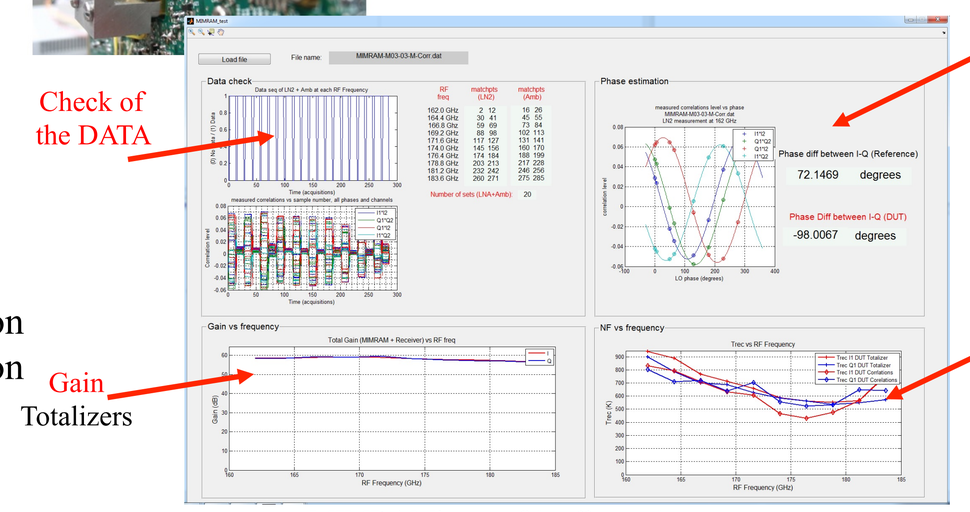

MIMRAM's user friendly environment

Method: Correlation, same technique used in the real instrument (basic unit or baseline). Requires knowledge of the reference receiver temperature, T_A (LN2, Amb), and attenuation of the hybrid coupler. Measurement at 10 different frequencies of the correlation deflection proportional to the temperature of the DUT.

91 % of MIMRAMs tested / 7 min per measurement

Conclusions: The basic elements of the system such as: antenna array (9 manifolds or 144 antennas), 36 IF boards, LO power distribution have been tested and assembled. The FPGA correlator testing method was selected as the main method to test the MIMRAMs since the correlation is insensitive to gain fluctuations, and is possible measure the I-Q, NF and gain of the DUT from the correlation results with a single measurement. Ideal for test large number of devices. 91 % of the MIMRAMs have been measured taking 7 min per device. Main results of the Antenna + MIMRAM and Receivers are: Tr ~ from 500 K to 800 K +-10%, I-Q balance ~ 90 degrees +-10% degrees and gain ~ 60 dB +-10%. The ASIC (ADC & correlator) is under test.

National Aeronautics and Space Administration
Jet Propulsion Laboratory
California Institute of Technology
Pasadena, California

Acknowledgements This work has been carried out at the Jet Propulsion Laboratory, California Institute of Technology under a contract with the National Aeronautics and Space Administration.

www.nasa.gov

Poster No. T-8

National Aeronautics and Space Administration

Extraction of Organic Compounds from Martian Soil Simulants using Supercritical Carbon Dioxide

Heather McCaig (382J), Amanda Stockton, Marlen Menlyadiev (3220), Candice Crilly, Sam Wright (382J), Ying Lin (4210), Isik Kanik (3220), and Fang Zhong (382J)

Project Overview

Mars In-Situ Organic Detection Instrument Using Supercritical CO_2 (SCCO2) Extraction

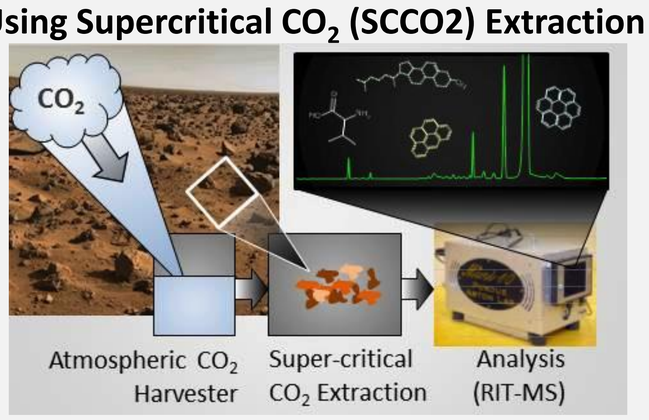

Challenges of Pyrolysis-Based Extraction

- Pyrolysis-based extraction methods require elevated temperatures.
- Perchlorate salts are present in Martian regolith at ppth level.[1]
- Organics may degrade in the presence of perchlorates at elevated temperatures.[2,3]
- Native organics may not be identified.[4]

Major Project Goals

- Extract organics under gentle SCCO2 conditions to prevent thermal degradation or reaction with native perchlorate salts.
- Analyze extracts with mass spectroscopy.
- Extract and detect compounds at ppb to ppt level.

Target Compound Classes

- Polycyclic aromatic hydrocarbons (PAHs)
- Amines and amino acids
- Hydrocarbons
- Fatty acids
- Steroids

MSSS/JPL-Caltech/NASA

Regolith samples could be procured by scooping, or other methods.

Supercritical CO_2 Extraction

Benchtop Extractor: Developing Experimental Protocols

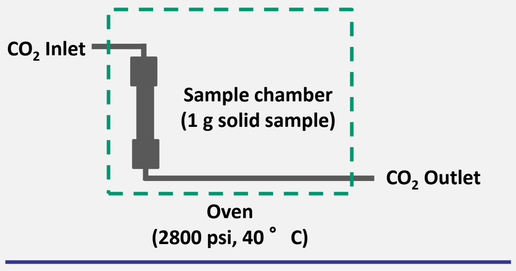

1) 5 min static extraction)
2) 20 mL CO_2 dynamic extraction

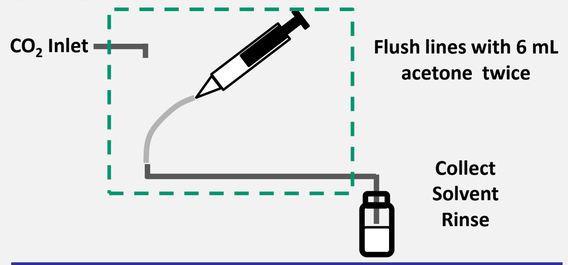

1) Rinse post-chamber lines to collect extract
2) Rinse substrate to collect residue
3) Quantify extract using analytical instruments

Martian Regolith Simulants

- Methods being developed for spiking with non-volatile and semi-volatile compounds.
- Typical concentrations: 1 ppb – 100 ppm.

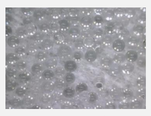

Glass micribeads (250-500 um) used as inert substrate

JSC Mars-1 Palagonite tephra from Hawaii

PAHs with Perchlorate Salts

SCCO2 Extraction of Coronene

PAHs are ubiquitous. Detection of PAHs or degradation products may indicate chemical processes present in Martian regolith[6,7] and provide information about the habitability of the surface and sub-surface.

- Coronene is representative of PAH compounds.
- UV-Vis indicates coronene does not degrade if extracted in presence of perchlorate.
- Perchlorate salt is not extracted with SCCO2.
- Extraction results in un-degraded, desalted sample, ready for analysis.
- SCCO2 extraction in presence of perchlorate will be expanded to other compounds.

Extraction Efficiency of Coronene Unchanged

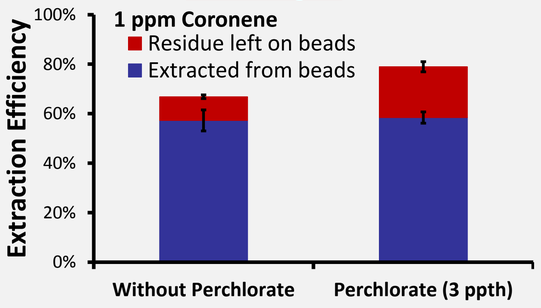

UV-Vis Spectra of Coronene Peak--Shape Unchanged

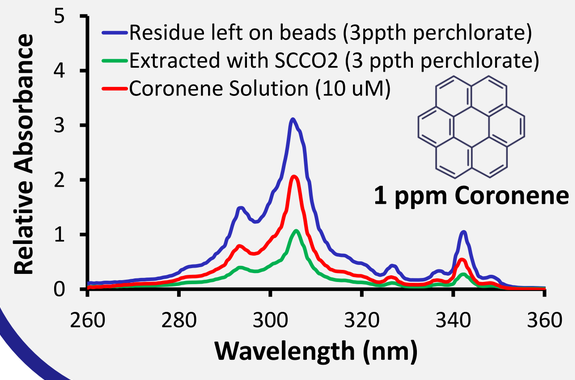

Perchlorate Salt Not Extracted

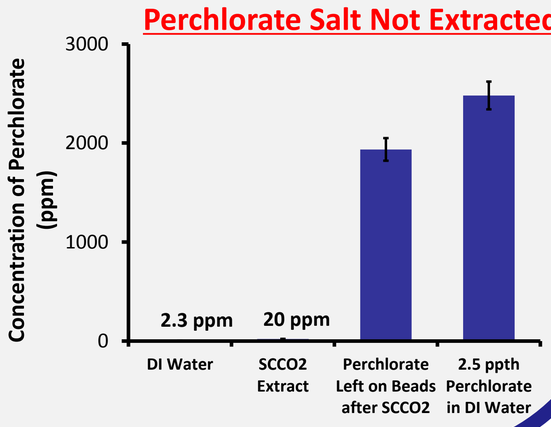

Biomarkers of Life and Habitability

Long-Chain Amines

- Ratio of different amines in dirt can indicate biotic or abiotic origin.
- Extracted samples analyzed with capillary electrophoresis with laser induced fluorescence (CE-LIF).[5]
- Preliminary extraction of amine compounds from beads (50 ppm). Capable of ppb-level detection.

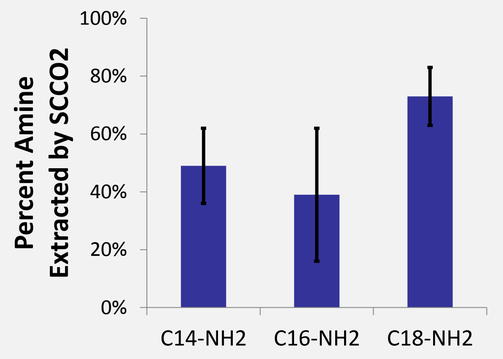

Carboxylic Acids

- As with amines, the pattern of different acids can indicate the existence of past/present life.
- Extracted samples analyzed with electrospray ionization mass spectroscopy (ESI-MS).
- Preliminary extraction of mixture of acids from beads (50 ppm each).

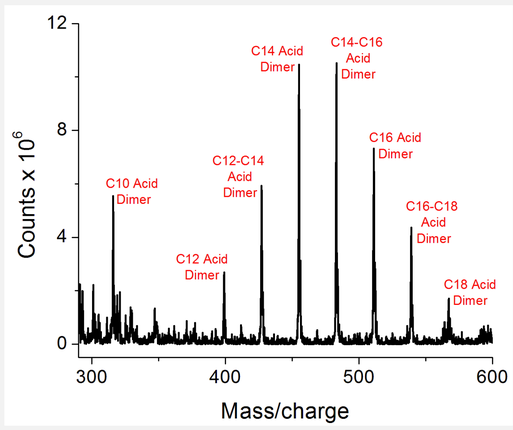

Extracting Native Compounds

A Step Towards Complex Samples

- 3D fluorescence spectra of JSC Mars-1 extracted with SCCO2 suggests extraction of a mix of native compounds at sub-ppb level.
- Addition of a separation technique would allow resolution of individual compounds.
- Indicates SCCO2 may be able to extract native, sub-ppb level organics from Martian regolith.
- May be more difficult to achieve with real Martian regolith if compounds are strongly bonded to the dirt.

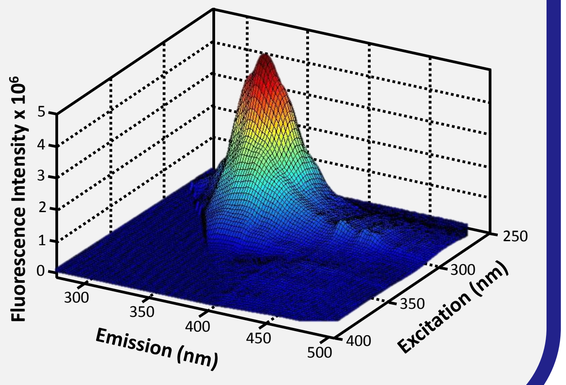

Conclusions

- Explored a variety of organic compounds with pure SCCO2 extraction.
- Perchlorate does not hinder extraction nor degrade extracted coronene.
- Infer extraction of trace native organics from Martian regolith simulant.
- Experiments indicate that SCCO2 extraction may overcome some of the challenges faced by previous pyrolysis extraction techniques used on Mars.

National Aeronautics and Space Administration

Jet Propulsion Laboratory
California Institute of Technology
Pasadena, California

www.nasa.gov

1. Hecht MH, Kounaves, SP, Quinn RC, West SJ, Young SMM, Ming DW, Catling DC, Clark BC, Boynton WV, Hoffman J, DeFlores LP, Gospodinova K, Kapit J, Smith PH, *Science* **2009,** 325, (5936), 64-67.
2. Ming DW, *40th Lunar and Planetary Science Conference. 2009. The Woodlands, Texas.: Lunar and Planetary Institute*, 2009.
3. Navarro-González R, Raine, FA, Molina P, Bagaley DR, Hollen BJ, Ros, JDL, Small AM, Quinn RC, Grunthaner FJ, Cácere, L, Gomez-Silva B, McKay CP, *Science* **2003,** *302* (5647), 1018-1021.
4. Stalport F, Glavin DP, Eigenbrode JL, Bish D, Blake D, Coll P, Szopa C, Buch A, McAdam A, Dworkin JP, Mahaffy P R, *Planetary and Space Science* **2012,** *67* (1), 1-13
5. Kendall CG, Stockton AM, McCaig HC, Chung S, Scott V, Zhong F, Lin Y, *J Anal Methods Chem* **2015**, Article ID 368362.
6. Clemett SJ, Dulay MT, Gillette JS, Chillier XD, Mahajan TB, Zare RN, *Faraday discussions* **1998,** (109), 417-436.
7. Flynn GJ*, moon, and planets* **1996,** *72*, 469-474.

Poster No. T-9

National Aeronautics and Space Administration

MgB_2 Mixers for Far-Infrared High Resolution Spectroscopy

Principal Investigator: Daniel Cunnane (389A)
Boris Karasik (389A)

Science Objective

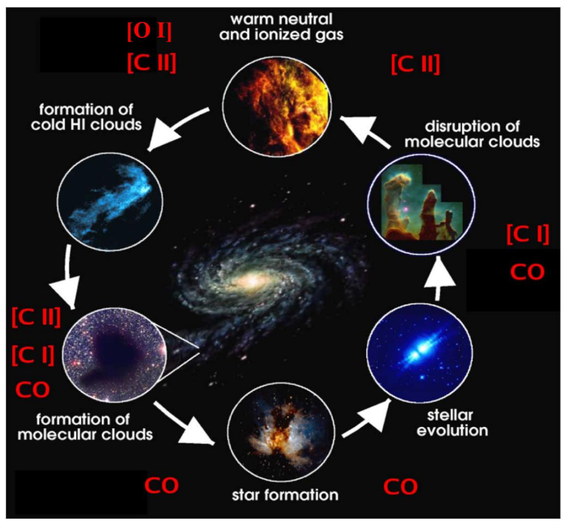

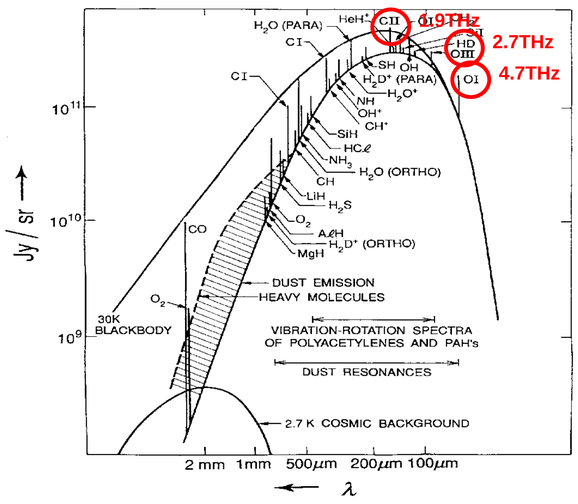

[CII] @ 1.9 THz and [OI] @ 4.7 THz are the major coolant lines for interstellar medium. Study of these lines gives information about the yet not well understood lifecycle of interstellar matter and astrochemistry of star forming regions.

Technology for Far-IR Heterodyne Spectroscopy

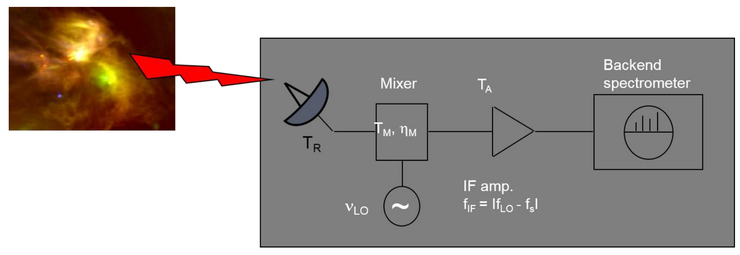

Mixing signal from the space object with a local oscillator allows for high spectral resolution ($\Delta\lambda/\lambda$ around 10^6).

NbN Hot Electron Bolometer (HEB) Mixers

Quasi-Optical Mixers For Herschel HIFI

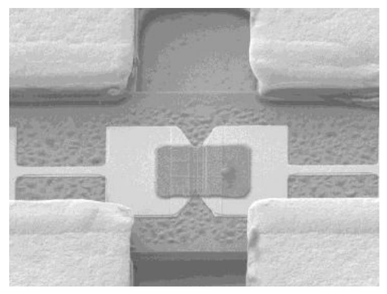

NbN mixer mounted in a Waveguide Block

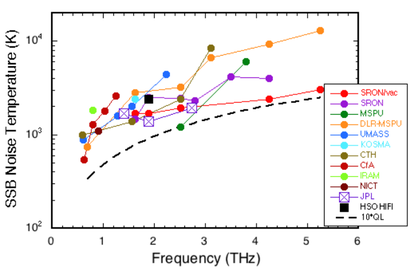

SOA IF Bandwidth of 2-3 GHz

Obstacles and Limitations

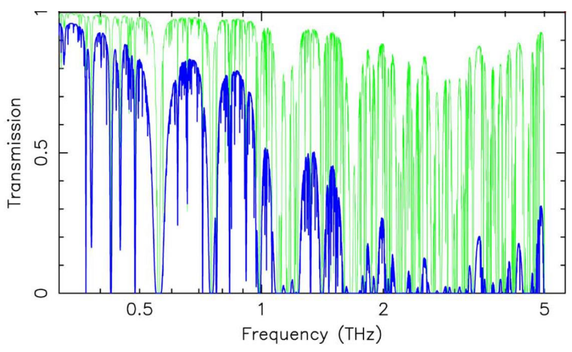

Atmospheric absorption of THz Radiation limits ground based observations (blue). Airborne platforms such as SOFIA or STO have better access to space (green) but space-based platforms like Herschel are ideal.

Operating temperature of NbN HEB devices requires liquid helium, which limited the Herschel mission duration to about 3 years.

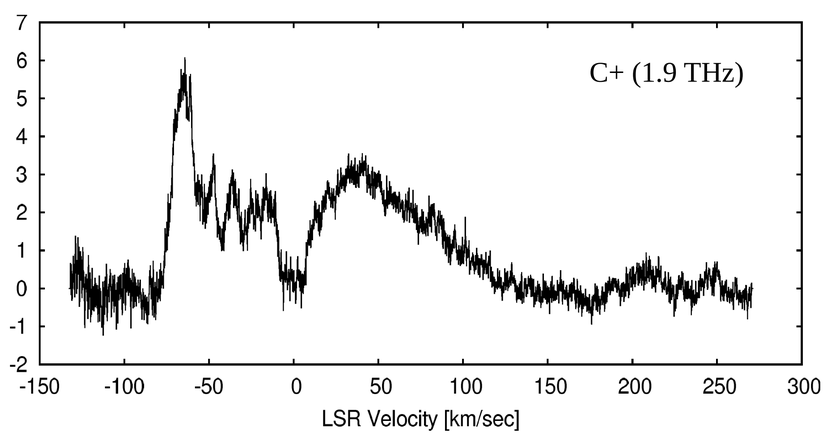

- Using Herschel HIFI, a scan of the galactic center at 1.9 THz had features spanning 450 km/sec using 3 GHz IF bandwidth.
- $\Delta f = \frac{\Delta v}{c} f_0$, Doppler broadening
- A similar scan for the 4.7 THz OI line would require over 7 GHz bandwidth to obtain the same velocity span. Larger IF bandwidth is necessary.

MgB_2 Mixers

Josephson Mixers

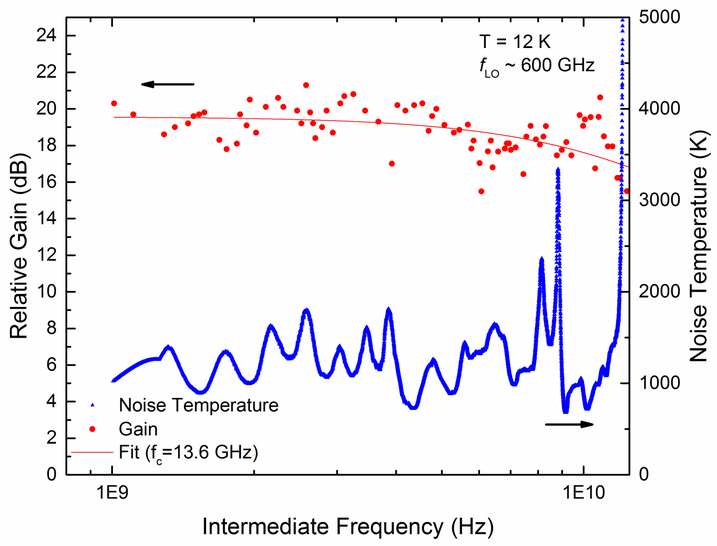

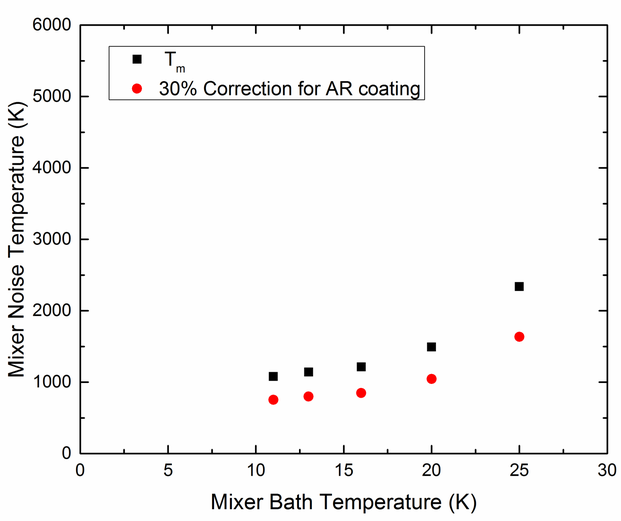

Josephson Mixer has potential to observe lines up to 2.5 THz. Low noise operation can be up to 20 K. The IF bandwidth is limited only by IF circuits components (> 10 GHz) and backend spectrometer.

Hot Electron Bolometer Mixers

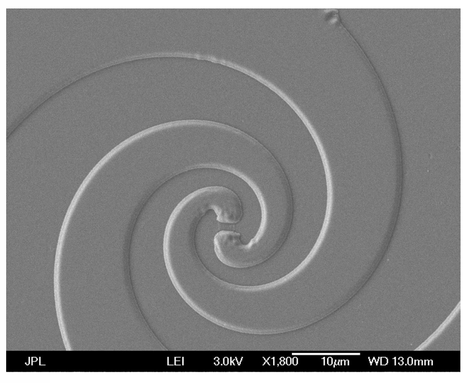

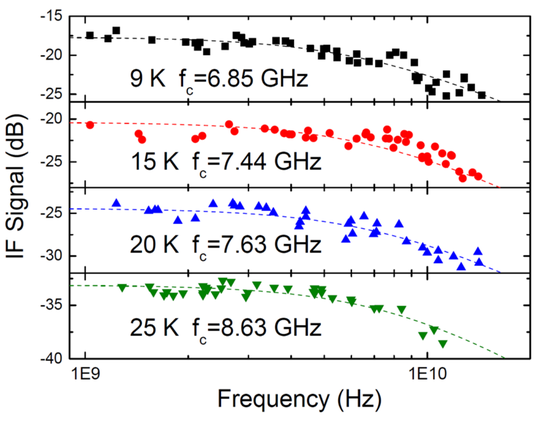

MgB_2 HEB Mixer has IF bandwidth verified to be 2.5 times larger than state of the art NbN HEB devices. Mixing has been demonstrated up to 25 K.

Conclusion: MgB_2 Mixers offer an alternative to NbN HEB mixers that can use low power cryocoolers for space-based missions while offering an increased IF bandwidth which is needed for [OI] spectral mapping.

National Aeronautics and Space Administration

Jet Propulsion Laboratory
California Institute of Technology
Pasadena, California

www.nasa.gov

Poster No. T-10

THz Heterodyne Array Development for Suborbital Missions

Principal Investigator: Jenna Kloosterman (389A)
Jonathan Kawamura (389A), Robert Lin (389A), Fahouzi Boussaha (Observatoire de Paris), Jose Siles (389A), Bruce Bumble (389I), Choonsup Lee (389A), Imran Medhi (389A)

Introduction

Key Science Goal:

Understanding the lifecycle of clouds of gas and dust in the Interstellar Medium (ISM)

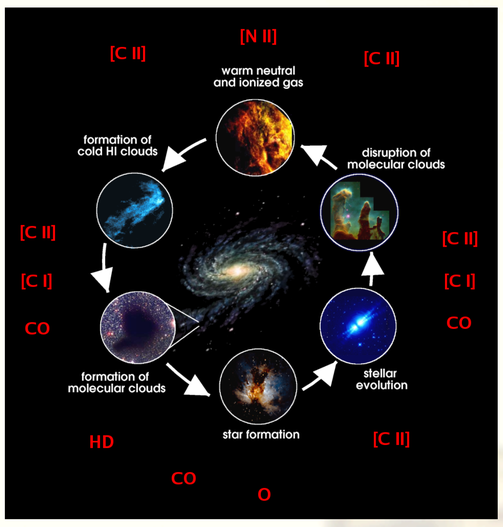

Image credit: Craig Kulesa and Chris Walker

Heterodyne receivers mix photons of different frequencies to:
- Maintain wave coherence
- Provide high spectral resolution ($\nu/\Delta\nu \geq 10^7$)
- Provide high sensitivity

THz (defined as 0.3-3 THz) heterodyne receivers require the development of:
- Local Oscillator (LO) sources
- Mixers

THz heterodyne arrays are needed to:
- Detect atomic and molecular tracers of the lifecycle of the ISM including CO, N^+, C^+, and O
- Increase mapping efficiency
- Disentangle large scale structures of gas clouds

Water absorption in Earth's atmosphere requires that most astronomical observations above ~1 THz be taken from orbital or suborbital platforms including airplanes, balloons, and spacecraft.

4-Pixel Array Receiver Configuration

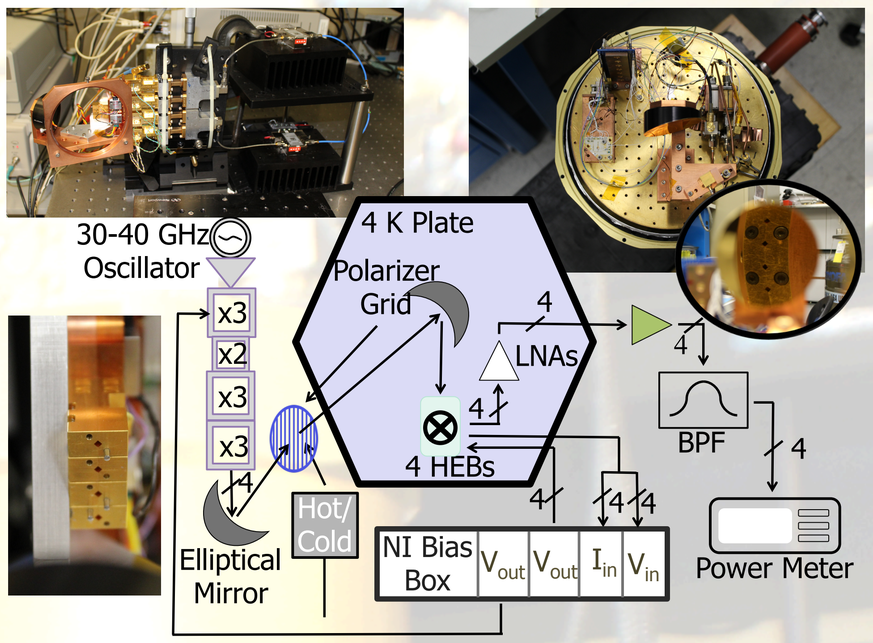

Local Oscillator: 4-Pixel Multiplier Chain

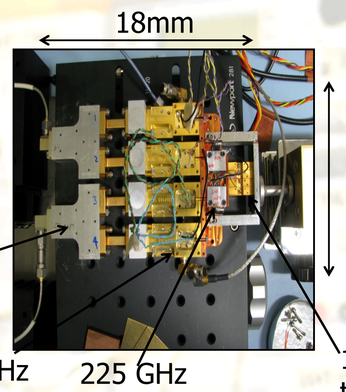

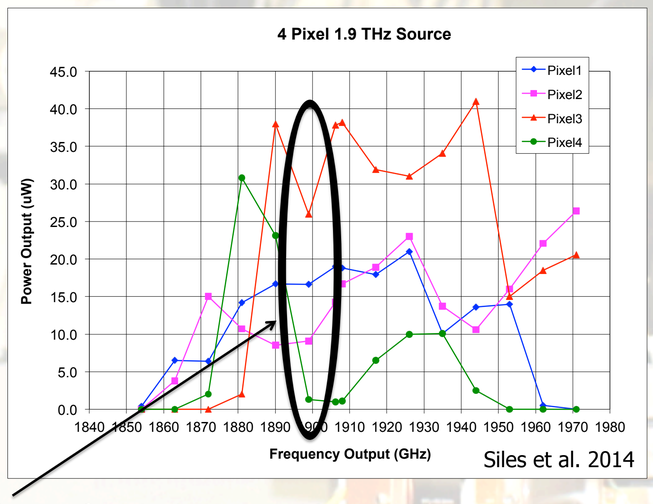

3 out of 4 pixels output 10+ μW of power, the amount needed to sufficiently pump the mixer at the target frequency

Results

	Ω_{RT}	$I_C(\mu A)$	$V_{BIAS}(mV)$	$I_{BIAS}(\mu A)$	$T_{RX}(K)$
Mixer 1	126	90.2	0.78	13.8	TBD
Mixer 2	114	89.6	0.69	8.6	840
Mixer 3	102	105.4	0.46	11.8	875
Mixer 4	0	NA	NA	NA	NA

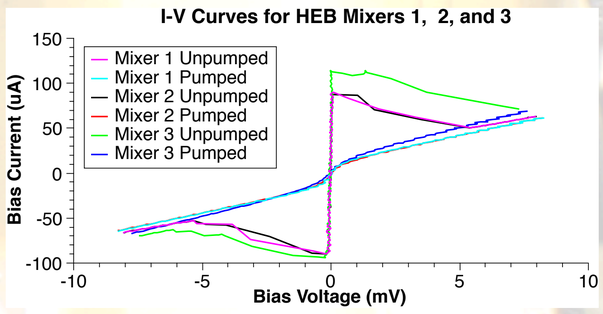

- Simultaneous pumping of Mixers 2 and 3, the maximum number of pixels supported by the current cryostat configuration. Mixer 1 was measured separately and Mixer 4 is shorted.
- Mixers showed maximum sensitivity at frequencies slightly lower than the target frequency
- In single pixel tests, 2nd generation HEB mixer design shows improvement with maximum sensitivity at the target frequency

Mixer: Hot Electron Bolometer (HEB)

- Superconducting mixer requires T_b < ~10 K
- Application of electrical bias and optical pumping from an LO source maintains a temperature distribution of "hot" electrons producing a resistive state at the center of the bridge
- Incoming signals modulate temperature causing a modulation in resistance.
- 4-pixel mixer block prototype fabricated with high precision Kern Machine
- Diagonal feedhorns have 5 mm spacing
- Full height waveguide designed for the C^+ line at 1.9 THz

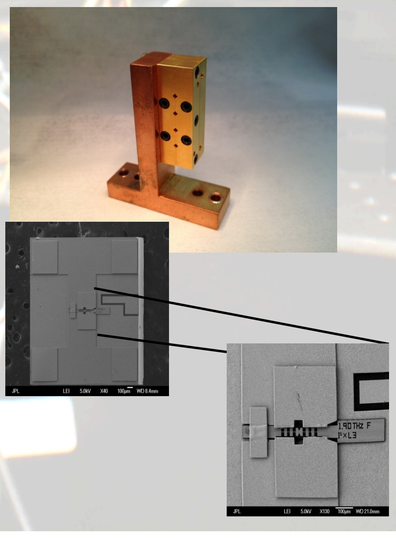

Conclusions and Future Work

- Newly designed Picket-Potter feedhorns with a circular to rectangular waveguide transformer demonstrate similar noise characteristics and reduce complexity in the design and fabrication process
- Beam pattern measurements of these Picket-Potter horns are underway to verify beam waist predicted by HFSS and CST simulations
- 2nd generation HEB mixers designed for the Stratospheric Terahertz Observatory 2 (STO-2) display maximum sensitivity at the target frequency of 1.9 THz
- Design is scalable to other frequencies such as 1.46 THz for N^+
- These new designs can be extended into larger arrays such as 4x2 or 4x4 by stacking the 4x1 LO and mixer blocks
- Planning Antarctica Long Duration Balloon flight with 4x1 arrays in December 2015!

National Aeronautics and Space Administration
Jet Propulsion Laboratory
California Institute of Technology
Pasadena, California

National Aeronautics and Space Administration

Superconducting Nanowire Detectors Based on MgB_2

A. E. Velasco[1], D. P. Cunnane[1] , R. M. Briggs[1] , A. D. Beyer[1] , M. D. Shaw[1] , B. S. Karasik[1] , M. A. Wolak[2] , N. Acharya[2] , X. X. Xi[2] , F. Marsili[1]

1) Jet Propulsion Laboratory, California Institute of Technology, Pasadena, CA 90242, USA
2) Temple University. Philadelphia, PA 19122, USA

Motivation

Superconducting nanowire single photon detectors (SNSPDs) perform single photon counting in the near IR with the best performance to date. However, state-of-the-art SNSPD technology is based on low critical temperature superconductors (LTS) operating at below 4 Kelvin for optimal performance. These requirements make LTS SNSPDs impractical for ground and flight applications where the required cryogenics is **expensive, complex, and high size, weight and power (SWaP).** Areas which would benefit from high-critical-temperature (T_C) SNSPDs are: quantum optics, quantum key distribution, quantum information, ranging (LIDAR), remote sensing (DIAL), deep-space optical communication, and quantum communication.

Single photon detection with SNSPDs[1]

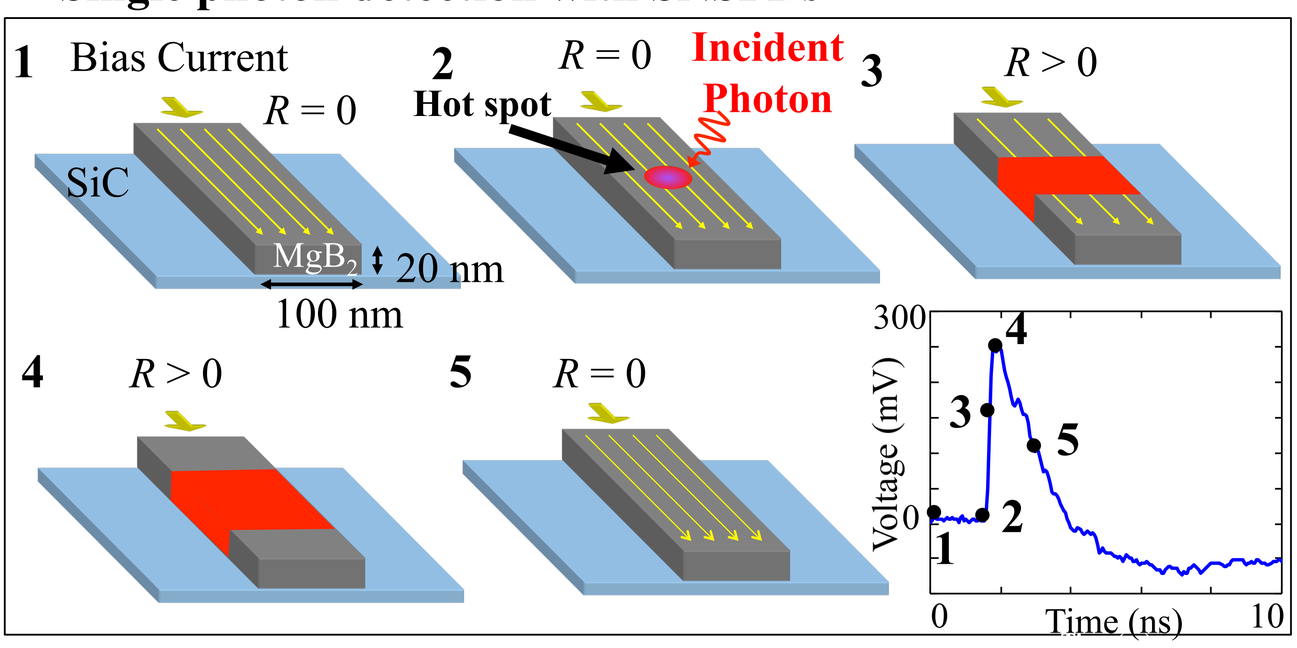

Challenges fabricating MgB_2 SNSPDs

1) High quality MgB_2 thin films difficult to grow

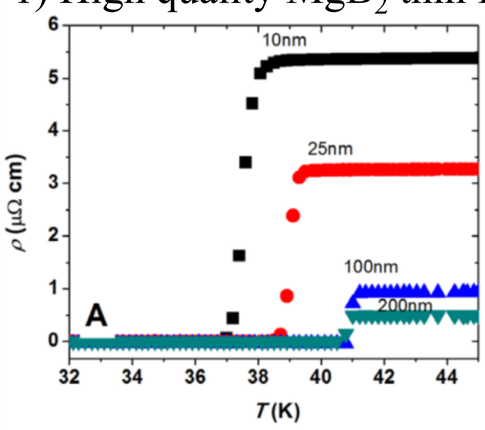

- Collaboration with Temple University, which fabricates the highest-quality MgB_2 thin films by HPCVD[2].
- Superconducting properties retained down to 10 nm-thick films.

2) MgB_2 readily oxidizes

- We are working to minimize air exposure to our samples and perform in-situ cleaning.

3) Etching limited to argon ion milling. Ar ion milling preferentially etches smaller features (~100 nm) over larger features.

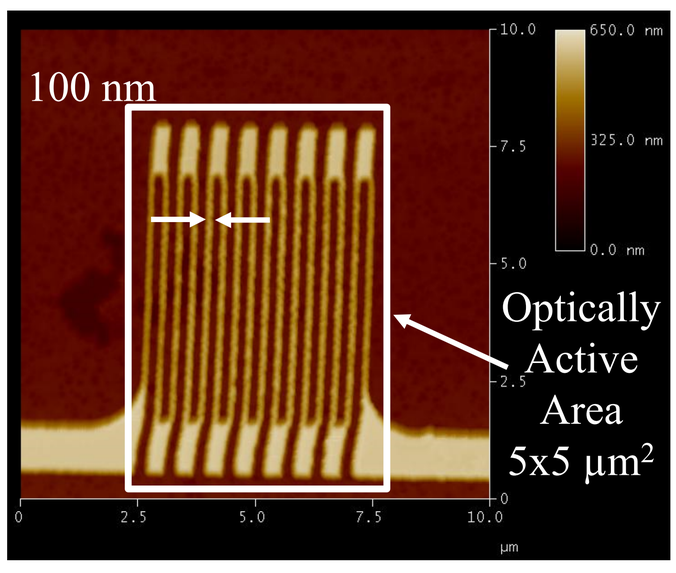

- Increased resist thickness to 400 nm.
- Minimized ion milling time by using inductively coupled plasma (ICP) etch.

Objective

Our objective is to demonstrate SNSPDs operating above 20 K where cryogenics is: **inexpensive, reliable, and low SWaP**. To achieve this goal we are developing high-T_C SNSPDs using the metallic superconductor magnesium diboride (MgB_2). The high bulk T_C (40 K) of MgB_2 could theoretically yield thin-film devices with single-photon-counting capability at 25 K. Our strategy is to fabricate SNSPDs at JPL using high-quality MgB_2 thin films deposited at Temple University by hybrid physical-chemical deposition (HPCVD).

Fabrication Process

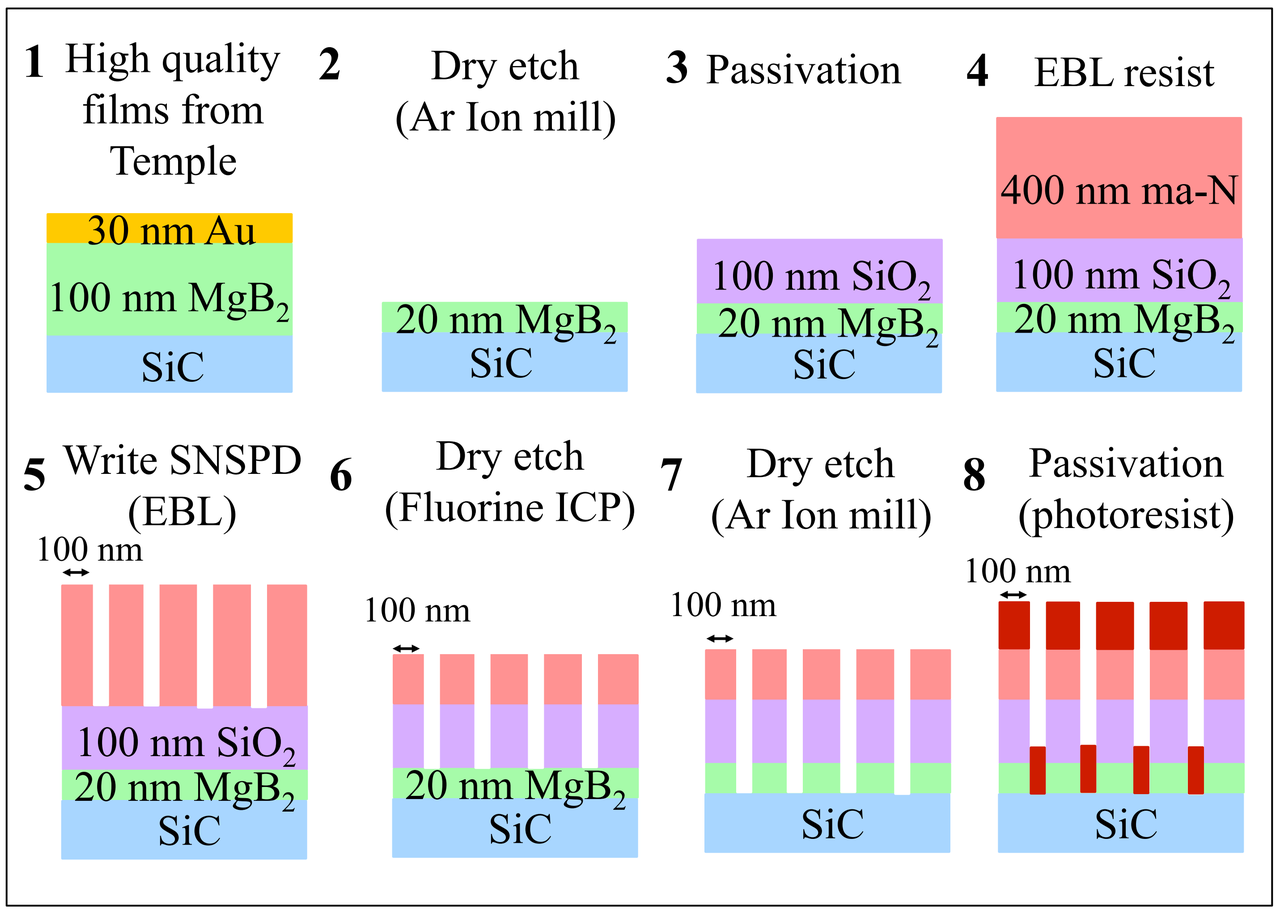

Preliminary Results: width 100 nm, thickness 20 nm

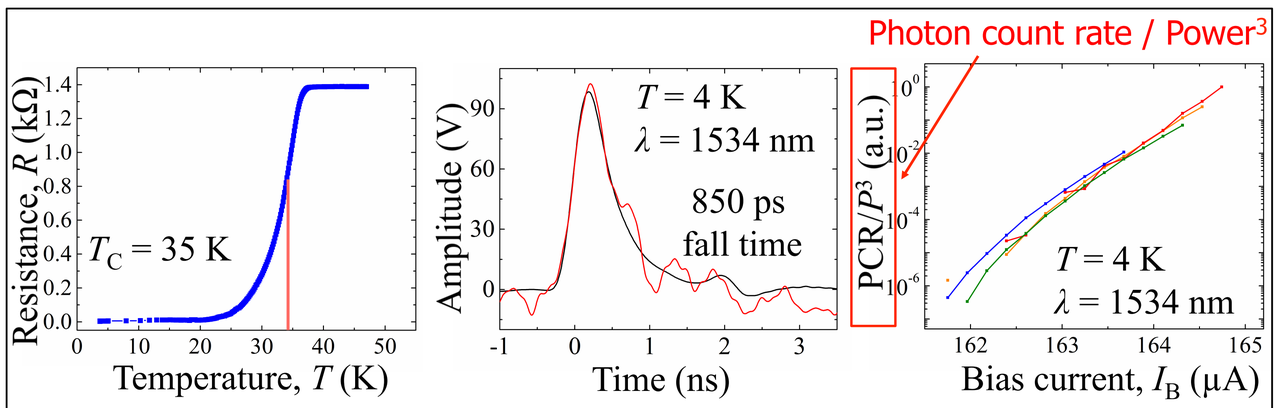

- Highest T_C of an MgB_2 nanowire to date
- Sub-nanosecond response
- No latching
- Three-photon sensitivity at 1534 nm
- Implies single photon sensitivity at 511 nm

Conclusion

Our fabrication work has yielded promising preliminary results: (1) highest T_C (35 K) for an MgB_2 nanowire to date, (2) cubic power dependence indicating three-photon sensitivity, and (3) sub-nanosecond photoresponse without latching to the resistive state. Remaining work is to achieve single photon sensitivity and increase the detection efficiency. We are working on fabricating thinner (~ 5 nm thick) nanowires which are expected to show increased photon sensitivity, and integrating the devices into an optical cavity to increase the detection efficiency.

References
1)Gol' tsman *et al.*, APL 79, 705 (2001)
2)C. Zhuang *et al.*, Supercond. Sci. Technol. **23** (5), 055004 (2010)

Poster No. T-12

National Aeronautics and Space Administration

Quantum capacitance detectors at the photon noise limit

Brian Pepper (389I)

Charles Bradford (3263), Theodore Reck (389A), Peter Day (389I), Kristjan Stone (382K), Daniel Wilson (389G), **Pierre Echternach (389I)**

Quantum capacitance detectors

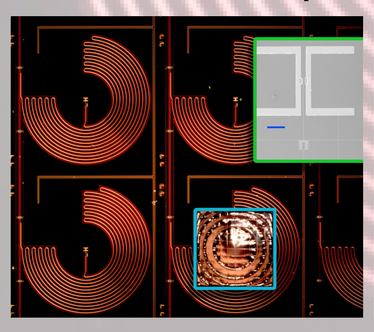

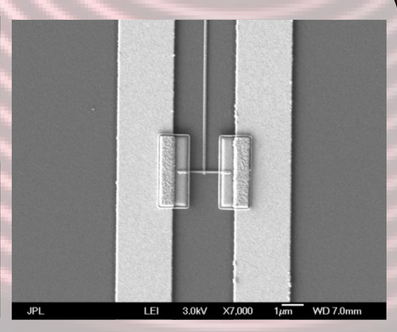

- Far-IR/THz detector based on single Cooper pair box
- Demonstrated NEPs below 10^{-21} W/Hz$^{1/2}$ @ 1.5 THz
- Demonstrated photon shot noise limited scaling @ 1.5 THz
- But…in original design, low optical efficiency (~3-4%)

Capacitively coupled QCDs

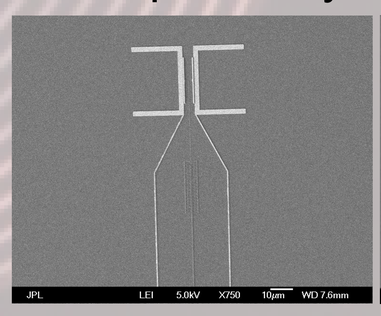

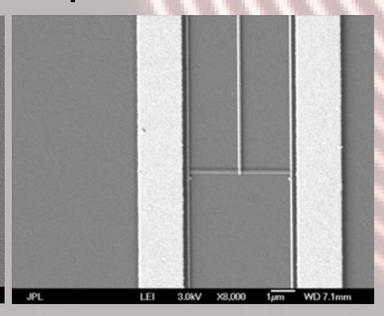

Replace Nb plugs with capacitors:
- Quasiparticles tunneling out while above Nb gap?
- Improve confinement of quasiparticles?

Sensitivity

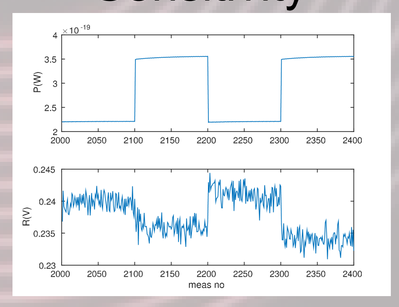

- When tuning temperature back and forth, can easily distinguish between very low background powers
- Currently lowest NEP of any THz detector

Principle of operation

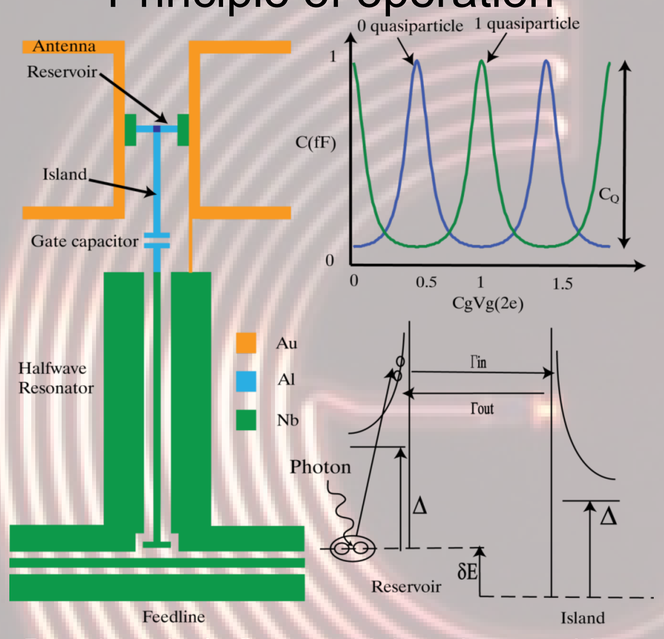

- Based on single Cooper pair box charge qubit
- Incoming photons break Cooper pairs in reservoir, creating quasiparticles
- Island normally in even state, but can be "poisoned" by quasiparticle tunneling over Josephson junction
- At degeneracy point, quantum capacitance alters resonance frequency of λ/2 microwave resonator

Response

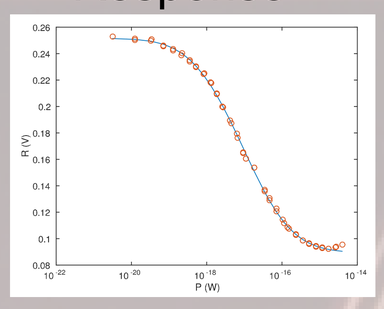

- Tune temperature of black body from 4.2 K to 40 K to alter illumination
- Resulting response curve is described by detailed balance equations for population of reservoir:

$$\frac{dN_{qp}}{dt} = \Gamma_{phot} + \Gamma_{gen} - RN_{qp}(N_{qp} - 1) - KN_{qp}p_{even} + \Gamma_{out}p_{odd} \quad (1)$$

$$\frac{dp_{odd}}{dt} = KN_{qp}p_{even} - \Gamma_{out}p_{odd}, \quad (2)$$

Telegraph rate asymmetry

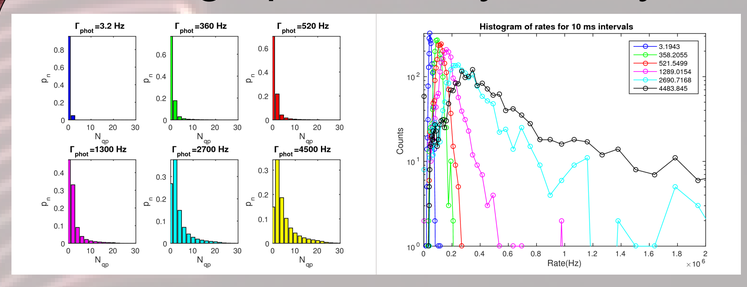

- Simulation of full master eqn, shows arrival of photons creates ~20 quasiparticles (QPs)
- Creates asymmetry in distribution of QP number
- This should translate to asymmetry in telegraph rate
- Qualitatively similar asymmetry is observed
- With higher bandwidth and slower recombination, might be able to observe single photon events!

Noise

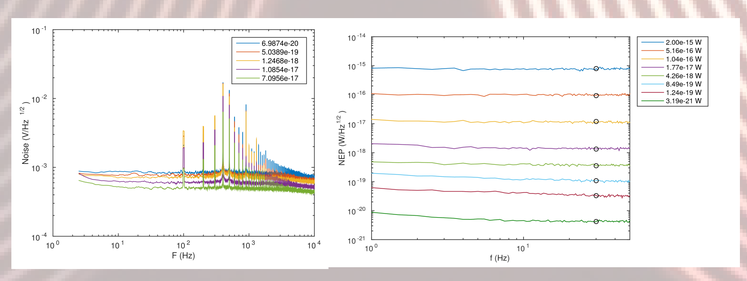

- Gate sweep at 100 Hz over 4 quantum capacitance peaks
- Shows 400 Hz peak and harmonics spaced 100 Hz apart
- By demodulating main peak, can recover signal

Conclusions

- Capacitive coupling improves □ from ~3% to 30-35%
  - Quasiparticles better confined?
- Photon shot noise limited scaling maintained
- Photon noise behavor @ lower powers w/ FFTs
  - Std. dev. method is 0.5 Hz measurement
  - FFT is 30 Hz measurement
  - TLS noise?
- Minimum NEP below 10^{-20} W @ 1.5 THz
- Telegraph rate asymmetry provides independent evidence of photon noise
- With higher bandwidth and larger reservoirs, single photon counting may even be possible.
- Strong candidate for future far-IR/THz space missions

Modes of operation

Degeneracy point

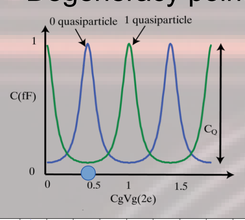

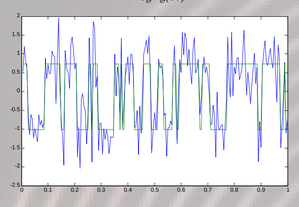

Gate sweep

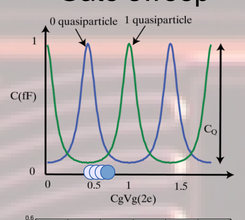

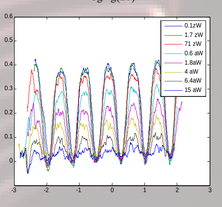

- If the gate voltage is tuned to the degeneracy point, the telegraph signal of quasiparticles tunneling in and out is visible.
- In a real array of devices, not possible to tune all to degeneracy simultaneously. Instead, sweep gate voltage so all devices can be read.

Noise Equivalent Power

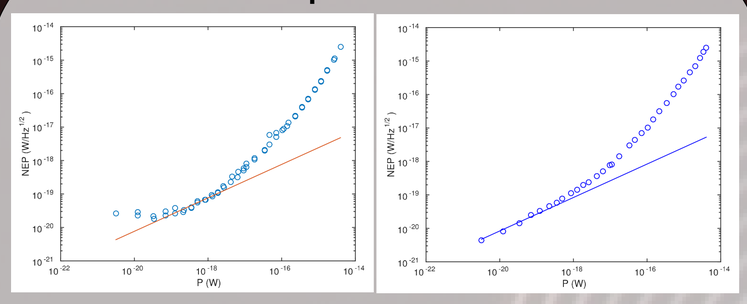

- Left graph shows plot of Noise Equivalent Power using standard deviation method
  - Photon shot noise limited from 10^{-19} W to 10^{-18} W
  - Effectively 0.5 Hz measurement: limited by TLS noise?
- Right graph shows plot of Noise Equivalent Power using standard deviation method
  - Photon shot noise limited from 3×10^{-21} W to 10^{-18} W
  - Effectively 30 Hz measurement

Future directions

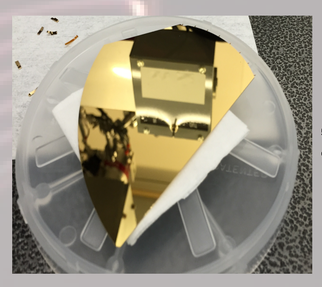

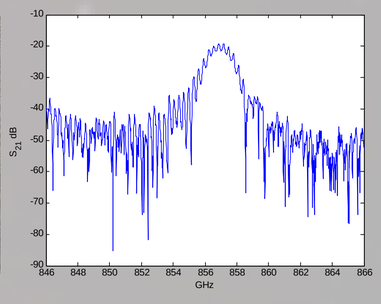

- Scale up: currently 5x5 arrays. Want: 100s!
- Begin integration with concept silicon immersion grating spectrometer in early testing
- Goal: R=500 spectrometer on a single 4-inch Si wafer
- Would enable future far-IR space missions with need for NEP below 10^{-20} W/Hz$^{1/2}$

National Aeronautics and Space Administration

Jet Propulsion Laboratory
California Institute of Technology
Pasadena, California

www.nasa.gov

Poster No. T-13

National Aeronautics and Space Administration

Planetary magnetic field sensing through "defective" silicon carbide microelectronics

Principal Investigator: Corey J. Cochrane (389K)
Jordana Blacksberg (389K), Gerardo Hernandez (1211), Neil Murphy (1211)
Jet Propulsion Laboratory, California Institute of Technology

1. Project Overview

- Development of a self-calibrating, solid-state magnetometer for planetary field sensing.
- The technology exploits the magnetic nature of unpaired electrons associated with atomic scale defects in Silicon carbide (SiC) microelectronics.
- Applications: planetary entry probes, landers, missions in extreme environments, and in swarms of spacecraft significantly smaller than current nanosats.

2. Magnetometers used in Space

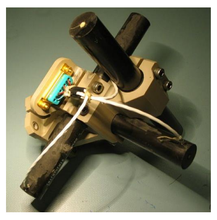

Courtesy NASA/THEMIS

Search Coil:
Application: AC fields, vectorized
Sensitivity: $\sim pT's/\sqrt{Hz}$
Missions: THEMIS, Pioneer 1/5, Explorer 6

Courtesy NASA/MAVEN

Ring Core Fluxgate:
Application: DC fields, vectorized
Sensitivity: $100's\ of\ pT/\sqrt{Hz}$
Missions: MAVEN, MGS, Messenger, Voyager 1/2, Mariner 2/4/5/10, Juno

Courtesy NASA/Pioneer 10/11

Optically Pumped Helium:
Application: DC fields ,vector, scalar
Sensitivity: $10's\ of\ pT/\sqrt{Hz}$
Missions: Cassini, Pioneer 10/11, Ulysses, SWARM, Europa (ICEMAG)

3. Advantages of New Concept

- Inexpensive, simple, small, and lightweight
- Solid-state, purely electrical, and low power
- Self-calibrating via electron nucear hyperfine interactions
- No temperature dependent, high frequency components
- No searching for a resonant signal, no dead zones
- Wide bandgap sensor: rad-hard, high temp environments
- One sensor needed for simultaneous monitoring of 3 axes
- Magnetic field modulation: eliminates 1/f noise, prevents DC current drift, sharp zero-crossing, vectorized field sensing, observation of electron-nuclear hyperfine interaction for self-calibration.

4. SiC Sensor(s)

- Wide bandgap (> 3eV): high temperature operation and inherently rad hard
- 4H or 6H crystalline polytypes allow for a relatively sharp response
- Ion implantation doping creates intrinsic atomic scale defects useful for field sensing
- Dopant/acceptor atoms create magnetic fingerprints used for self-calibration

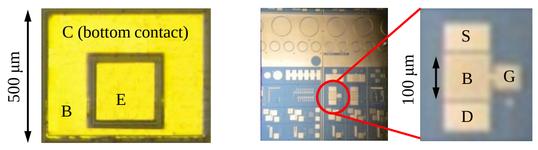

(a) 4H SiC BJT (b) 4H SiC/SiO_2 nMOSFET

5. Theoretical Operation: Zero-field Spin Dependent Recombination

- Atomic scale defects have broken bonds that contain unpaired electrons which have intrinsic angular momentum called spin.
- Conduction electrons may couple with these defect spins which sometimes results in recombination with a hole if angular momentum is conserved between the spin pair. See panel (a).
- In an applied magnetic field, one can change the recombination rate by randomizing the spin pair orientations, either by application of EM energy (resonant SDR) or removing the magnetic field (zero-field SDR). See panel (b).

(a) Generalized process of Spin Dependent Recombination (SDR) in a semiconductor.

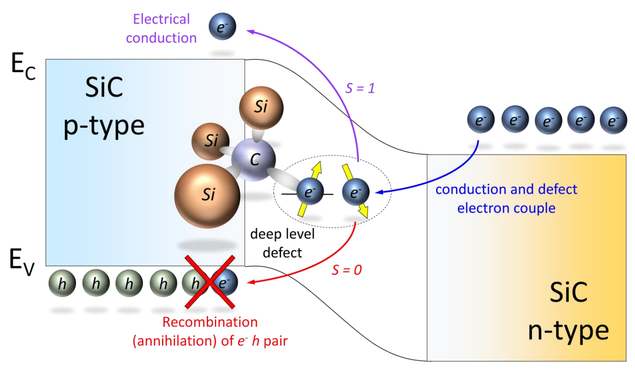

(b) Typical Electrically Detected Magnetic Resonance (EDMR) spectrum: SDR current versus magnetic field with constant EM energy applied

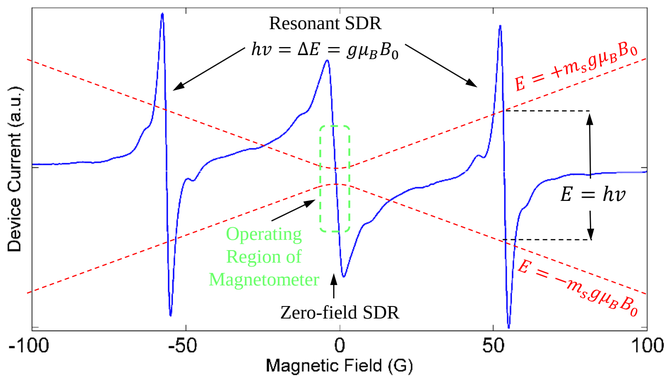

6. Signal Conditioning, Processing, and Control

- The (a) SiC sensor and signal conditioning circuitry is housed inside a (b) three axis set of Helmholtz coils which are independently controlled to maintain a local region of zero-magnetic field across the volume of the sensor.
- Each set of coils also serves to modulate the external magnetic field (orthogonal audio waveforms) which (c) frequency division multiplexes the three current components onto a single channel.
- The conditioned sensor current is digitized and fed through three independent software demodulators to extract the embedded current components
- A controller then tracks the zero crossing of these components and pumps each Helmholtz coil with the required current needed to maintain region of zero magnetic field across the sensor.

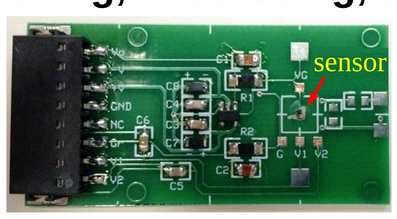

(a) Current conditioning circuitry

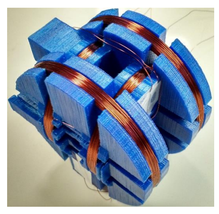

(b) 3D printed 3 axis Helmholtz coils

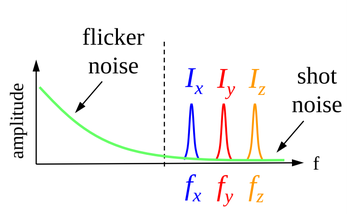

(c) Modulation channels

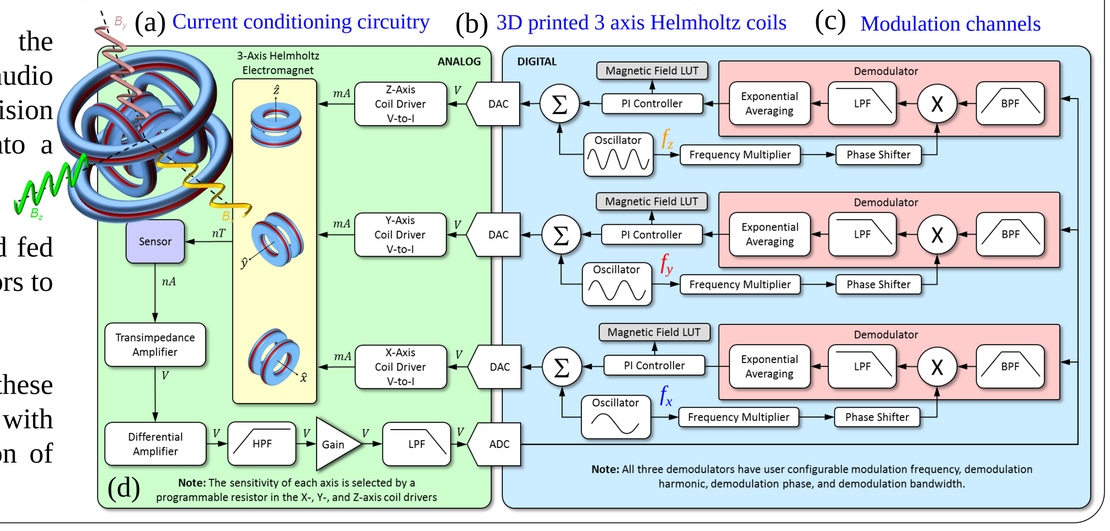

(d) Note: The sensitivity of each axis is selected by a programmable resistor in the X-, Y-, and Z-axis coil drivers

7. Predicted Sensitivity

The SDR current vs. field response can be assumed to be Gaussian,

$$I(B) = \frac{\Delta I}{\sigma\sqrt{2\pi}}\ exp\left\{-\frac{(B-B_r)^2}{2\sigma^2}\right\}\left(\frac{A}{T}\right)$$

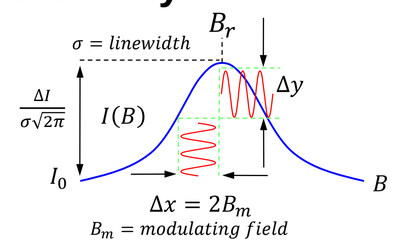

Because modulation is used, the measured data is

$$I_d(B) = \Delta y = \frac{dI(B)}{dB}\Delta x\Big|_{\Delta x = B_m}\left(\frac{A}{T}\right)$$

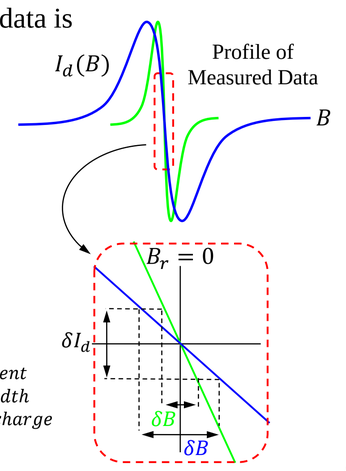

The local sensitivity is defined by,

$$\delta I_d(B) = \delta B\left|\frac{dI_d(B)}{dB}\right|_{B=0} = \delta B\frac{\Delta I}{\sigma^3\sqrt{2\pi}}{B_m}^2$$

Assuming shot noise, $\delta I_d = I_{shot} = \sqrt{2qI_0\Delta f}$

$$\frac{\delta B}{\sqrt{\Delta f}} = 2\sqrt{\pi q}\frac{\sigma^3}{{B_m}^2}\frac{\sqrt{I_0}}{\Delta I}\left(\frac{T}{\sqrt{Hz}}\right)$$

I_0 = DC current
Δf = bandwidth
q = electronic charge

Initial Goal~1 $nT\ \sqrt{Hz}^{-1}$

8. Initial Results

Comparison of the high-field SDR (detected via EDMR) and zero-field SDR current as a function of magnetic field for both (a) a 4H SiC BJT and (b) a 4H SiC MOSFET.

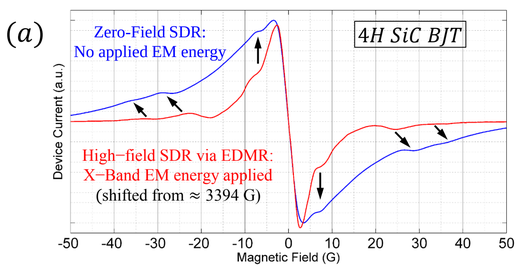

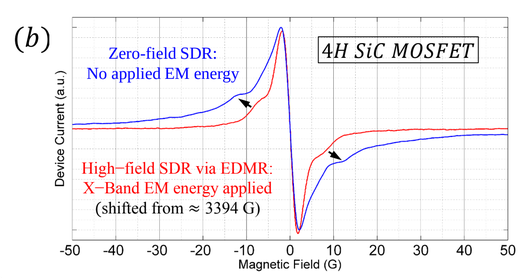

Panel (c-d) illustrate the 1st harmonics and panel (e-f) illustrate the 2nd harmonic zero-field SDR responses in the presence of three different fields as a function of magnet current for the SiC BJT and MOSFET, respectively. This data is proof of concept demonstration that there is much potential for near zero magnetic field sensing with SiC sensors.

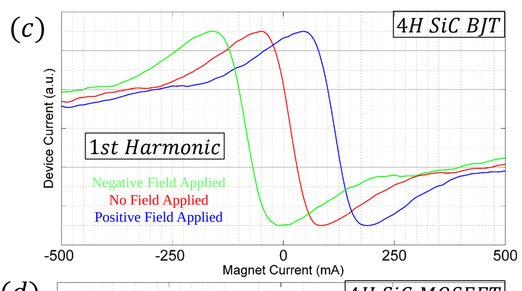

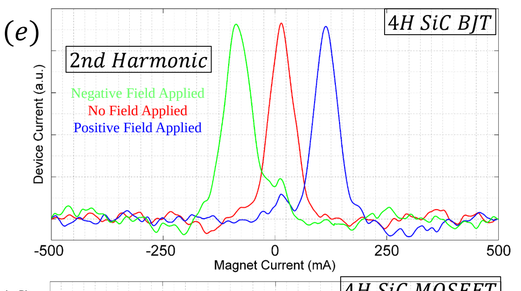

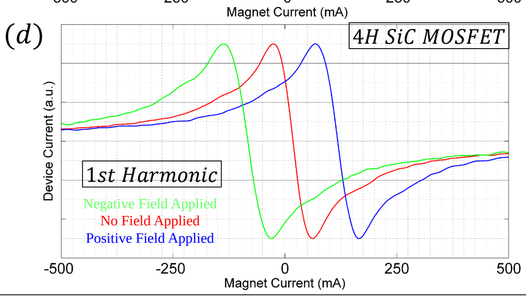

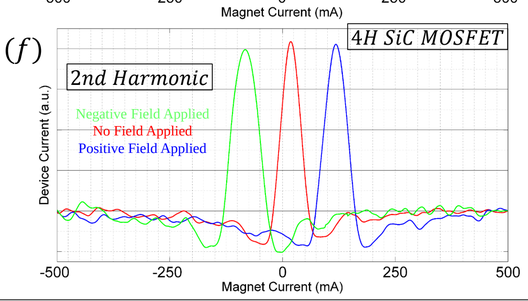

9. Next Steps

- Perform a trade study on SiC devices obtained from NASA Glenn, Cree, and Monolith Semiconductor which have various doping concentrations, annealing methods to find optimum sensor for magnetometer.
- Use defect engineering methods to develop a similar sensor that minimizes the ratio $\sigma\sqrt{I_0}/\Delta I$ to maximize sensitivity.
- Miniaturize magnetometer and measure performance.

10. Conclusion

- We've demonstrated a new solid state, vectorized magnetometer which has the potential to be miniaturized and used in high temperature and high radiation environments.
- These features enable the use of the technology in variety of magnetic field sensing applications, including planetary entry probes, landers, missions in extreme environments, and in swarms of spacecraft significantly smaller than current nanosats.

National Aeronautics and Space Administration
Jet Propulsion Laboratory
California Institute of Technology
Pasadena, California

www.nasa.gov

Poster No. T-15

National Aeronautics and Space Administration

Increasing MSL & ChemCam science return by optimizing autonomous target selection

Raymond Francis (398),
Tara Estlin (398), Daniel Gaines (397), Benjamin Bornstein (398), Steven Schaffer (397), Vandi Verma (347)

Curiosity will soon choose its own science targets

ChemCam

The Mars Science Laboratory's (MSL) ChemCam instrument includes the first-ever Laser-Induced Breakdown Spectrometer (LIBS) on a planetary mission, as well as a Remote Micro-Imager (RMI) context camera. It provides **standoff geochemical measurements** at up to 7 m range, and this capability has proven valuable **for survey and triage** of targets for more detailed and resource-intensive follow-up activities. Over 200,000 measurements have been made since MSL's landing in August 2012. With its narrow field of view, ChemCam **relies on target selection** to obtain data from the most scientifically valuable features.

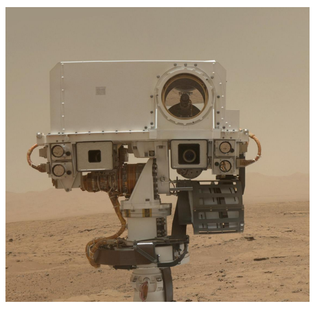

Top: The ChemCam aperture on MSL's mast. **Above:** ChemCam LIBS marks on a Martian target.

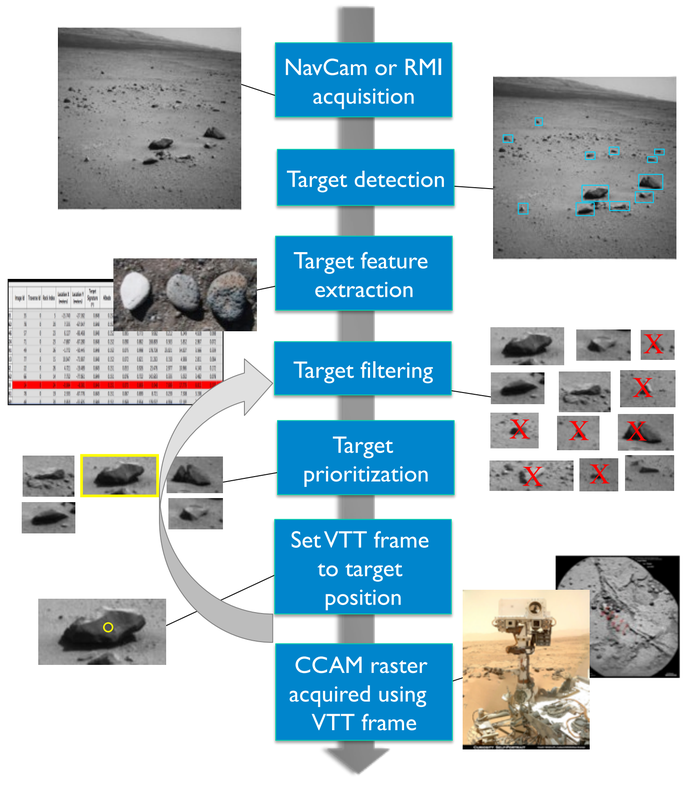

AEGIS

JPL's *Autonomous Exploration for Gathering Increased Science* software suite allows a rover to **autonomously find and select targets** in navigation camera images, and target science instruments at them. AEGIS has been operational on the *Opportunity* rover since 2010, where it has allowed PanCam images to be collected **without the delay incurred by waiting for humans on Earth** to pick the targets in transmitted imagery (which can be 1-4 days, typically). This **increases both science return and efficiency** of the mission. This unprecedented capability in autonomous, intelligent science target selection by a robotic system earned AEGIS the award for NASA software of the year in 2011. AEGIS will soon be deployed aboard *Curiosity* to choose targets for ChemCam.

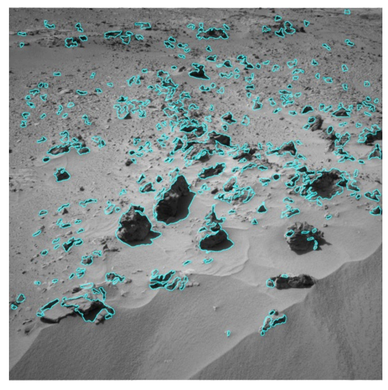

Above: Rock targets identified in an MSL NavCam image, before filtering & ranking.
Left: Autonomous targeting process using AEGIS. The process can loop back to the filter step, to acquire several observations with different target signatures during a single execution, all without ground personnel in the loop.

Teaching a robot what's important: the *Target Signature*

Geology

What makes a good target? What do geologists want to find to answer the mission's science questions?
The search for past habitable environments hinges on understanding the geologic history of Gale Crater and its sediments. The science team must identify the **different geological units** present, find their **boundaries**, and understand their **physical relationships**. Recognizing each unit, variations and small-scale features within it, and its contacts with other units, are key visual tasks supporting this survey and interpretation work.

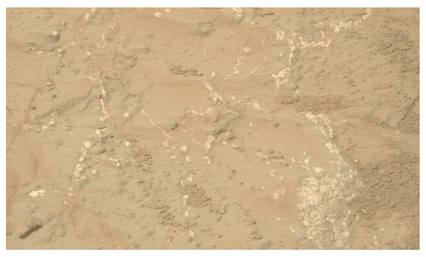

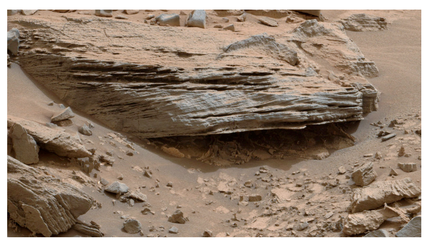

Top: Veins in the Knorr target at Yellowknife Bay **Above:** Cross-bedding in the Whale Rock target at Pahrump Hills. Each provided clues that led to a decision to drill nearby, as at the John Klein site **(Right)**

Computer vision

How can a computer recognize a geological target? Which computer-vision 'features' are diagnostic of geological materials?
AEGIS can recognize, filter, and rank targets based on a number of parameters, all built from the tools of digital image processing. Pixel **intensity, size, shape, statistical uniformity**… these kinds of features are easily extracted. Teaching AEGIS to recognize a geological material requires understanding that material's visual expression, and **determining the combination of features** that correspond to each type of geological target of interest.

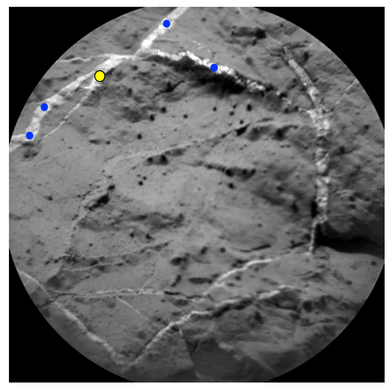

Above: Cued on pixel intensity, AEGIS identifies the top five positions for a ChemCam raster to study veins. The RMI image is overlain with a yellow mark at the top candidate, and blue marks at the runners-up. Combinations of features can give signatures for other types of targets.

Easier operations, more and better science data

Parameter templates

Rather than require the science team to tune AEGIS each day during tactical planning, templates of **parameters for each geological setting** in the rover's work area are being developed. **Tuned to the types of targets most desired by the science team**, they will be implemented in MSLICE, the science team's operations planning software.

Above right: ChemCam scientists choose targets using NavCam imagery. When this is not (yet) available, AEGIS templates will allow them to easily guide the rover to the desired types of targets in previously unseen locales.
Right: Each ChemCam activity (in pink) can be planned with a different target signature in MSLICE.

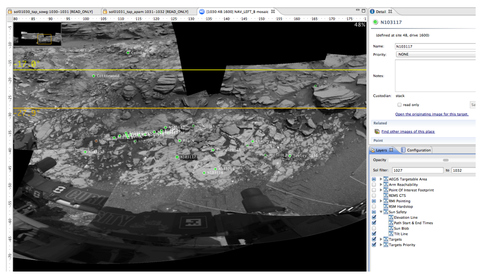

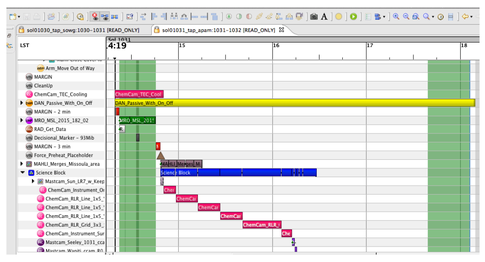

Benefits to MSL

- Find **higher-quality targets**, by improving the accuracy of AEGIS' target-ranking output
- **Lighten the task load** of the science operations team
- Enable **more frequent use of ChemCam**, especially during periods of limited data return to support target selection ('restricted sol periods')
- **Speed the overall mission progress** by delivering geochemical survey data faster – at the same time as the drive-completion data is received

Future steps

Near term: Curate the templates
- **Adapt templates** in response to performance on Mars, and changing conditions
- Add new templates as the rover encounters **new geological units** and features

Farther out: **Mars 2020**
- Adapt the system to **new instruments**, especially ChemCam's successor, **SuperCam**
- **Efficient mission progress** will be important for the ambitious sample-collecting mission; AEGIS can **save command cycles and mission time**.

National Aeronautics and Space Administration
Jet Propulsion Laboratory
California Institute of Technology
Pasadena, California

www.nasa.gov

Raymond Francis is a Visiting Post-Doctoral Fellow at NASA's Jet Propulsion Laboratory. His work is primarily funded by his home institution, the Centre for Planetary Science and Exploration (CPSX) at the University of Western Ontario, through a fellowship from the CREATE network for Techniques and Technologies for Earth and Space Exploration, supported by the Natural Sciences and Engineering Research Council of Canada.

Poster No. T-17

National Aeronautics and Space Administration

Spatial Statistical Estimation for Massive Sea Surface Temperature Data

Investigator: Yuliya Marchetti (398L)
Jorge Vazquez (329D), Hai Nguyen (398L), Amy Braverman (398L)

Goals

- Spatial prediction (i.e. estimation) for **massive** datasets and **ultra high resolution** prediction (e.g. 1km).
- Combine measurements from any number of **different** sources with different biases, measurement errors and footprint sizes.
- Provide an estimated **uncertainty** of the predicted values.

Methodology

Spatial Statistical Data Fusion (SSDF)

SSDF is a flexible spatial prediction in a statistically rigorous way, which minimizes uncertainty by exploiting **global** spatial correlations in the data. SSDF provides uncertainty estimates for the predictions, accounts for the measurement errors and biases, and scales to large datasets through a dimension reduction mechanism:

— Each observed measurement ($\mathbf{Z}$) is a linear combination of a true process ($\mathbf{Y}$) and a measurement error (ϵ).

— True process ($\mathbf{Y}$) can be further decomposed into a large scale trend (μ), small scale spatial structure (ν) and fine scale variability (ξ).

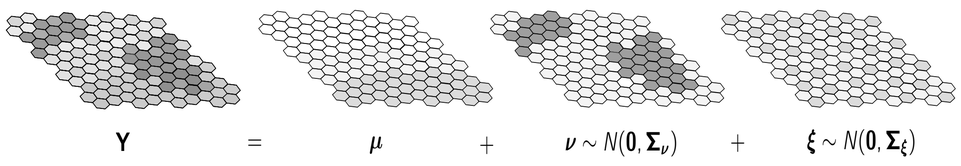

$$\mathbf{Y} = \mu + \nu \sim N(\mathbf{0}, \mathbf{\Sigma}_\nu) + \xi \sim N(\mathbf{0}, \mathbf{\Sigma}_\xi)$$

— Small scale spatial structure (ν) represents a low-dimensional data space (i.e. spatial random effects) and allows handling of massive datasets.

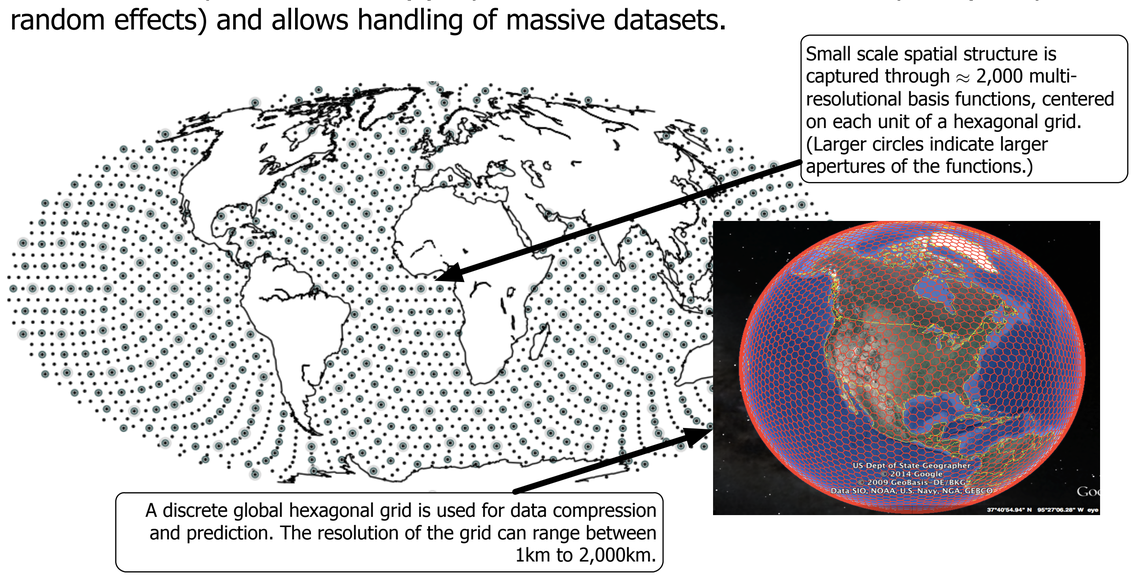

Estimation — computing model covariance parameters Σ_ν and Σ_ξ

- Obtained parameters are **global**.
- Measurements are aggregated to coarse hexagonal grid with 30km resolution, since estimated parameters have considerably fewer dimensions than data.
- Maximize Gaussian likelihood function over the parameters given the data using Expectation-Maximization algorithm.

Prediction — finding true process ($\mathbf{Y}$) in any new location

- The predicted values are obtained for each unit of the hexagonal grid on any resolution in any region or the full globe.
- The high resolution prediction is performed over an area of interest (full globe can be done blockwise or in parallel) but using data globally.
- **Adaptive multi-resolution grid** uses full information content in the area of interest and nearby. Remote locations contribute less information and provide further dimension reduction.

Application To Sea Surface Temperature (SST)

High resolution prediction (≈ 1km) of SST is important for science applications, especially in critical parts of the oceans, such as coastal upwelling regions:

- Combine infrared (MODIS, VIIRS) and microwave (AMSR-2) measurements to achieve better coverage under clouds and rainfall.
- SST data is massive — about 30-50 million measurements twice daily per infrared instrument and about 7 million for each microwave instrument.
- A global prediction per each time of day is about **500 million** locations for 1km resolution.

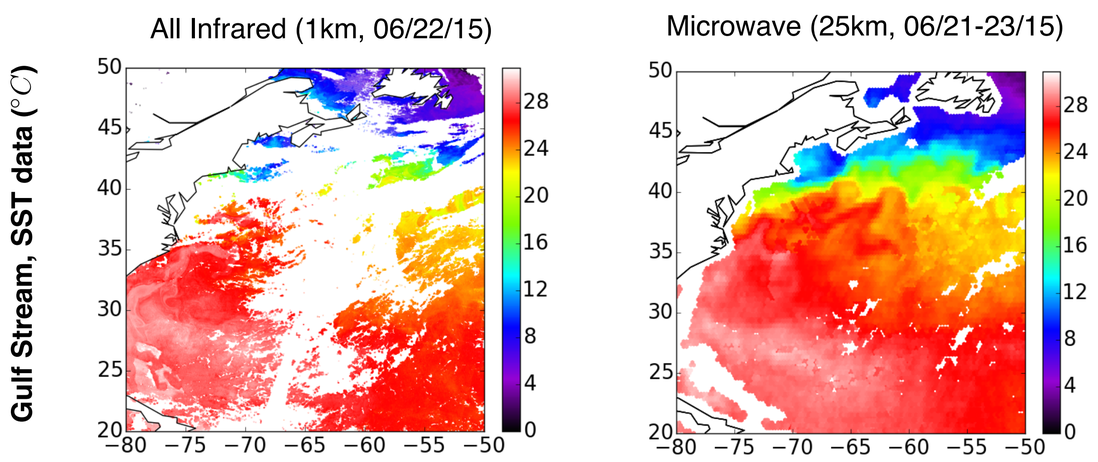

Predicted values for Gulf Stream region for 06/22/15, as (1) trend, (2) small scale structure, (3) fine scale variability, and (4) total predicted SST.

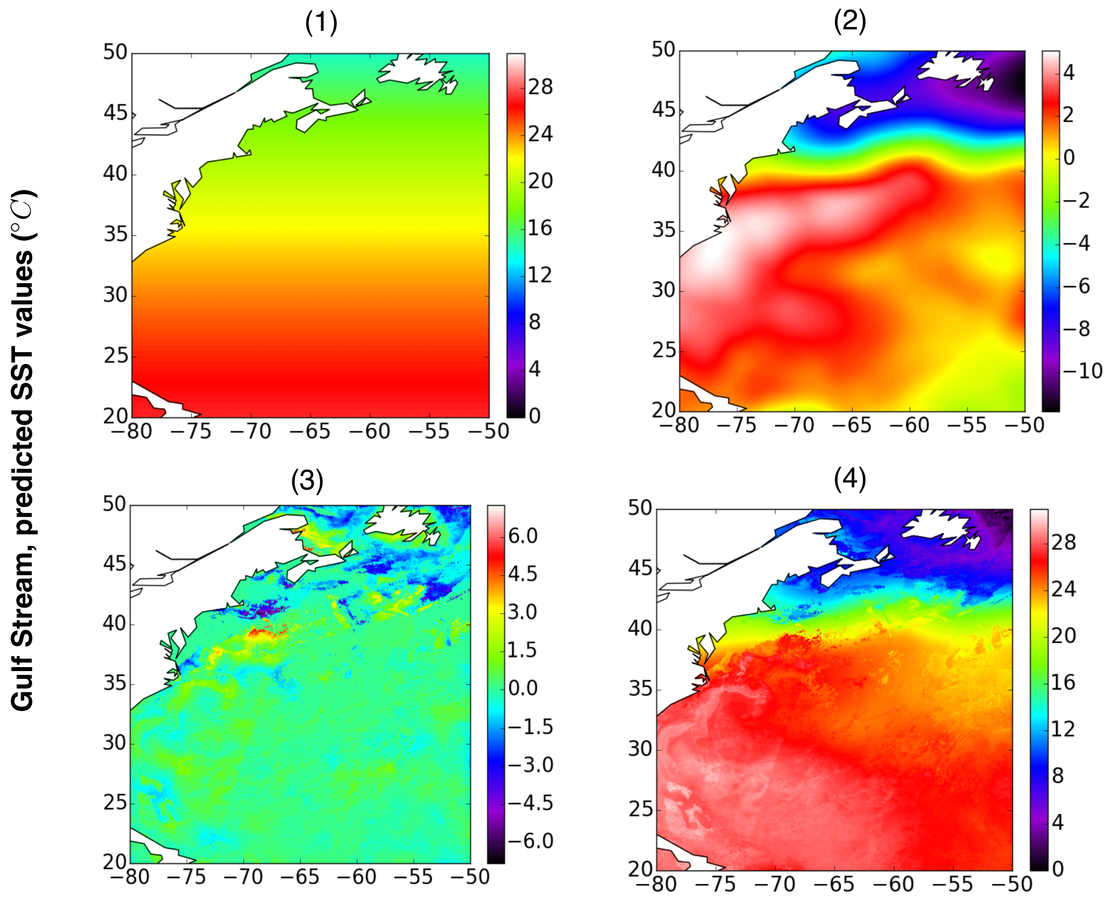

Future Work

- Implement Conditional Autoregressive Model for better quality of the prediction incorporating nearest neighbor information.
- Investigate resolution and information content of data as a function of distance.
- Explore the contribution of different instruments on prediction.
- Perform validation and comparison studies.

Uncertainty!

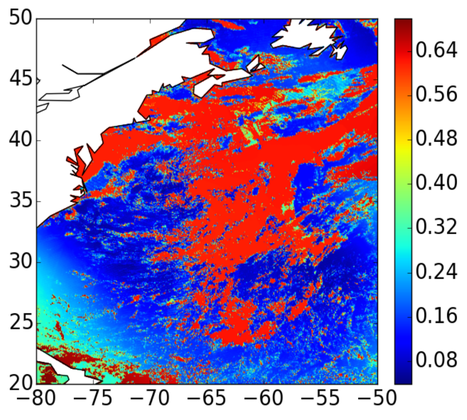

We are able to produce global high resolution datasets and to handle several massive remotely sensed SST datasets (over **100 million** data points) in a reasonably short time through dimension reduction and adaptive multi-resolution spatial grid.

National Aeronautics and Space Administration
Jet Propulsion Laboratory
California Institute of Technology
Pasadena, California

www.nasa.gov

Poster No. T-22